Involvement of miR-605 and miR-34a in the DNA Damage Response Promotes Apoptosis Induction

Chun-Hong Zhou,[†‡] Xiao-Peng Zhang,[†] Feng Liu,[†*] and Wei Wang[†*]
[†]National Laboratory of Solid State Microstructures, and Department of Physics, Nanjing University, Nanjing, China; and [‡]School of Physics and Electronic Engineering, Jiangsu Normal University, Xuzhou, China

ABSTRACT MicroRNAs are key regulators of gene expression at the posttranscriptional level. In this study, we focus on miR-605 and miR-34a, which are direct transcriptional targets of p53 and in turn enhance its tumor suppressor function by acting upstream and downstream of it, respectively. miR-605 promotes p53 activation by repressing the expression of *mdm2*, while miR-34a promotes p53-dependent apoptosis by suppressing the expression of antiapoptotic genes such as *bcl-2*. What roles they play in the p53-mediated DNA damage response is less well understood. Here, we develop a four-module model of the p53 network to investigate the effect of miR-605 and miR-34a on the cell-fate decision after ionizing radiation. Results of numerical simulation indicate that the cell fate is closely associated with network dynamics. The concentration of p53 undergoes few pulses in response to repairable DNA damage, or it first oscillates and then switches to high plateau levels after irreparable damage. The amplitude of p53 pulses rises to various extents depending on miR-605 expression, and miR-605 accelerates the switching behavior of p53 levels to induce apoptosis. In parallel, miR-34a promotes apoptosis by enhancing the accumulation of free p53AIP1, a key proapoptotic protein. Thus, both miR-605 and miR-34a can mediate cellular outcomes and the timing of apoptosis. Moreover, miR-605 and PTEN complement each other in elevating p53 levels to trigger apoptosis. Taken together, miR-605 and miR-34a cooperate to endow the network with a fail-safe mechanism for apoptosis induction. This computational study also enriches our understanding of the action modes of p53-targeted microRNAs.

INTRODUCTION

MicroRNAs (miRNAs) are noncoding RNAs 20–24 nucleotides long. They posttranscriptionally repress the expression of target genes by pairing to the 3′ untranslated region of messenger RNA (mRNA) and recruiting the RNA-induced silencing complex, which mediates the repression of translation and the degradation of the target mRNA (1). More than 30% of human protein-coding genes are regulated by miRNAs (2). miRNAs can confer robustness to biological processes by acting as buffers against random fluctuation in gene expression (3).

The tumor suppressor p53 is a central player in the cellular response to various stresses including DNA damage, hypoxia, and oncogene activation (4). Once activated, p53 selectively modulates expression of target genes involved in cell cycle arrest, DNA repair, and apoptosis (5). Besides protein-coding genes, p53 mediates the expression of miRNAs, including the miR-34 family as well as miR-192, miR-194, miR-215, miR-107, and miR-605 (6–9). p53 is also involved in the processing of miRNAs such as miR-16, miR-143, and miR-145 (10). It has been shown that miRNAs are important components of the p53 network and there exist intricate connections between p53 and its target miRNAs (11). How p53-targeted miRNAs contribute to its tumor suppressor function is still less well understood.

Recently, it was shown experimentally that p53 dynamics control cell fate (12). A series of computational studies have also explored the dynamics and functions of p53 in response to DNA damage. We proposed in previous articles that the cell-fate decision between survival and death after ionizing radiation (IR) can be determined by the number of p53 pulses (13,14) and that high plateau levels of p53 facilitate apoptosis induction (14). Choi et al. reported that different dynamic modes of p53, such as pulsing and sustained accumulation, are associated with distinct cell fates (15). However, the effect of p53-targeted miRNAs on cellular output is largely neglected in the modeling of p53 signaling. It is important to investigate what roles miRNAs may play in the p53-mediated DNA damage response (DDR). Meanwhile, it is necessary to justify the previously proposed mechanism for cell-fate decision in a wider context that includes the protein-miRNA interactions.

There are two kinds of p53-targeted miRNAs worth noting. The first can regulate p53 activity through repression of its negative regulators such as Mdm2 and wild-type p53-induced phosphatase 1 (Wip1) (9,16,17). For example, miR-605 represses Mdm2 posttranscriptionally (9). Thus, miR-605 can upregulate p53 via the p53-miR-605-Mdm2 positive feedback loop. The second kind of miRNA, including miR-34a, can function downstream of p53 to mediate cellular outcomes (18,19). The target proteins of miR-34a include Bcl-2, SIRT1, E2F3, CDK4/6, and Myc (20), and thus miR-34a promotes cell cycle arrest and apoptosis. For simplicity, we can choose miR-605 and miR-34a as representatives of these two kinds of miRNA

Submitted September 20, 2013, and accepted for publication February 26, 2014.

*Correspondence: fliu@nju.edu.cn or wangwei@nju.edu.cn

Editor: Reka Alber.

0006-3495/14/04/1792/9 $2.00

http://dx.doi.org/10.1016/j.bpj.2014.02.032

and probe how they cooperate to affect the DDR in a p53-dependent manner.

Motivated by the above considerations, here we develop a four-module network model of the p53 signaling pathway to explore the influence of miR-605 and miR-34a on p53 dynamics and cell-fate decision after IR. Consistent with our previous report (14), p53 undergoes one- or two-phase dynamics depending on the extent of DNA damage. miR-605 can accelerate the full activation of p53 to induce apoptosis, while miR-34a promotes the accumulation of free p53-regulated apoptosis-inducing protein 1 (p53AIP1), facilitating apoptosis induction. Therefore, the involvement of miR-605 and miR-34a ensures that severely damaged cells can be removed promptly. This work suggests that p53-targeted miRNAs play a critical role in p53 signaling; their effect on gene expression could be amplified via positive feedback and cascade response to elicit a large physiological effect.

MATERIALS AND METHODS

Model

p53 is at the center of cellular signaling pathways responding to various stresses (4). It is increasingly evident that miRNAs are important components of the p53 network (11,21). Here, we propose a four-module model for the p53 network in response to IR, focusing on the impact of miRNAs on the DDR. The model characterizes DNA repair, ataxia-telangiectasia mutated (ATM) activation, regulation of p53 activity, and determination of cellular outcome (Fig. 1). p53-centered feedback loops play key roles in shaping p53 dynamics and modulating p53 activity (22). We consider the p53-miR-605-Mdm2 and p53-PTEN (phosphatase and tensin homolog)-Akt-Mdm2 positive feedback loops, as well as the p53-Mdm2 and ATM-p53-Wip1 negative feedback loops. The key points of the model are presented as follows.

Induction, repair, and detection of DNA damage

Upon IR, double-strand breaks (DSBs) are induced, and DNA repair proteins are quickly recruited to break sites (23). For a population of cells exposed to the same irradiation dose, D_{IR}, the number of DSBs is assumed to obey a Poisson distribution with a mean of $35 \times D_{IR}$ (24). The total number of repair proteins is assumed to be 20/cell. We use the same method as Zhang et al. (14) to simulate the DSB repair process. Each DSB site may be in one of three states: intact, in complex with repair protein, and fixed, with the total number of sites in each state denoted by N_D, N_C, and N_F, respectively. Both fast and slow repair processes are taken into account. The two-lesion kinetic model is used to characterize the repair process (25).

As a detector of DSBs, the ATM kinase is activated via intermolecular autophosphorylation (26). ATM exists predominantly as dimers in unstressed cells. After IR, DSBs promote conversion of ATM from dimers to inactive monomers and to active, phosphorylated monomers.

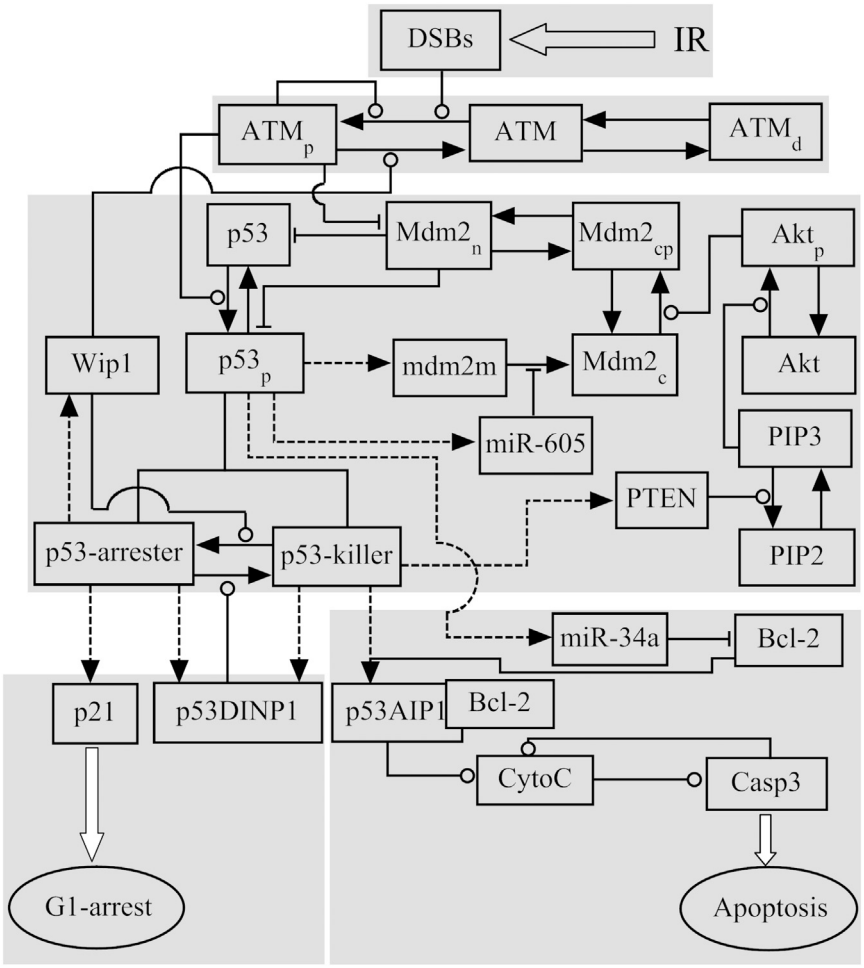

FIGURE 1 Schematic depiction of the model. DSBs are induced upon IR, and the ATM kinase is activated via autophosphorylation. Activated p53 induces the expression of *mdm2*, miR-605, and miR-34a. miR-605 and miR-34a repress the translation of *mdm2* and *bcl-2* mRNAs, respectively. Active p53 is further divided into p53-arrester and p53-killer, which promote cell cycle arrest and apoptosis, respectively. Dashed arrows denote the expression of target genes by p53, whereas solid arrows represent the transitions between proteins. Circle- and bar-headed lines denote the promotion and inhibition, respectively, of transition or production.

Phosphorylated ATM (ATM_p) further accelerates the activation of ATM through intermolecular autophosphorylation. Consequently, ATM_p becomes dominant and transmits the stress signal downstream by phosphorylating its substrates.

p53-mediated cell-fate decision

Activated ATM phosphorylates p53 and Mdm2, blocking the p53-Mdm2 interaction and promoting the rapid degradation of Mdm2 (27,28). As a result, p53 is stabilized and activated. Only nuclear p53 is considered here. Based on its phosphorylation status, p53 is divided into three forms: unphosphorylated (p53, the inactive form), phosphorylated on Ser-15 (p53-arrester, the primarily activated form), and doubly phosphorylated on Ser-15 and Ser-46 (p53-killer, the fully activated form) (13,14). Phosphorylated p53 is collectively symbolized by $p53_p$. p53-arrester and p53-killer induce cell-cycle arrest and apoptosis, respectively (29,30). Three forms of Mdm2 are considered: the dephosphorylated cytoplasmic form ($Mdm2_c$), the phosphorylated cytoplasmic form ($Mdm2_{cp}$), and the nuclear form ($Mdm2_n$). The *mdm2* mRNA, mdm2m, is also included in the model. We assume that only phosphorylated Mdm2 can enter the nucleus (31).

p53-arrester transactivates *p21*, *Wip1*, and *p53DINP1* (p53-dependent damage-inducible nuclear protein 1), whereas p53-killer transactivates *PTEN*, *p53AIP1*, and *p53DINP1* (29,30,32). p21 induces cell-cycle arrest, whereas p53AIP1 promotes apoptosis. We assume that the rate constant of p53DINP1 induction by p53-killer is much greater than that by p53-arrester, because p53-killer has a higher affinity for the promoter of *p53DINP1* than does p53-arrester (30). The conversion between p53-arrester and p53-killer is controlled by p53DINP1 and Wip1 (30,33). p53DINP1 promotes the accumulation of p53-killer via phosphorylation (30), whereas Wip1 promotes the reversion from p53-killer to p53-arrester via dephosphorylation (33).

Wip1 also promotes the dephosphorylation of ATM_p (34), and the ATM-p53-Wip1 negative feedback loop is essential for uniform p53 pulses in the DDR (35). PTEN promotes the conversion from phosphatidylinositol 3,4,5-trisphosphate (PIP3) to phosphatidylinositol 4,5-trisphosphate (PIP2) via dephosphorylation (36); PIP3 recruits Akt to the plasma membrane, promoting its phosphorylation (37). Phosphorylated Akt (Akt_p) phosphorylates cytoplasmic Mdm2 to trigger its nuclear entry (31). Thus, there exists a positive feedback loop comprising p53-killer, PTEN, PIP2/3, Akt, and Mdm2 (38).

Active p53 induces the expression of miR-605 and miR-34a. miR-605 suppresses the translation of *mdm2* mRNA (9). Thus, p53, miR-605, and Mdm2 constitute a positive feedback loop. miR-34a can promote cell-cycle arrest and apoptosis (20). Here, we focus on its proapoptotic function. miR-34a represses Bcl-2 posttranscriptionally. As an antiapoptotic factor, Bcl-2 inhibits p53AIP1 by forming a complex (39). Only free p53AIP1 induces the release of cytochrome *c* (CytoC) from mitochondria into cytoplasm. Released CytoC results in the activation of caspase-3 (Casp3) (40), and activated Casp3 further promotes CytoC release by cleaving its inhibitors (41). Consequently, apoptosis ensues. For simplicity, we do not explicitly consider the intermediate steps between CytoC release and Casp3 activation, including the formation of apoptosomes and activation of caspase-9 (42).

Methods

The details of model construction are presented in the Supporting Material. A Monte Carlo method (13,14,24) is used to mimic the DNA repair process. The concentration of each species is represented by a state variable in rate equations, which are presented in Supporting Material. Michaelis-Menten kinetics is used to characterize the reactions involving phosphorylation and dephosphorylation. All transcription of genes by p53 is characterized by the Hill function, and the Hill coefficient is set to 4 given the cooperativity of the tetrameric form of p53 as a transcription factor (43). The description of variables and their initial values are listed in Table S1. A set of standard parameter values is listed in Table S2. The unit of time is minutes, and irradiation dose is in units of Gray (Gy). The units of parameters are determined such that the concentration of proteins is dimensionless. For simplicity, we did not indicate the units of the parameters explicitly. Numerical integration of differential equations was performed using a fourth-order Runge-Kutta algorithm with a time step of 0.01 min. The bifurcation diagrams were plotted using Oscill8.

RESULTS

Typical dynamics of the p53 network

We first exhibit the dynamics of key proteins under two typical stress conditions. Upon IR, the number of DSB-protein complexes, N_C, rises quickly to its maximum of 20 and remains there until the number of DSBs drops below 20; after that, N_C falls gradually (Fig. 2). ATM is activated by the presence of DSBs, and p53 is then activated by ATM; the concentrations of ATM_p and $p53_p$ first undergo pulses. $p53_p$ induces p21 to arrest the cell cycle, allowing for DNA repair. At $D_{IR} = 2$ Gy, since the damage is effectively fixed after two p53 pulses, Casp3 remains inactive and the cell recovers to normal proliferation (Fig. 2 *A*).

At $D_{IR} = 6$ Gy, N_C is around the maximum for a long time (Fig. 2 *B*). $[ATM_p]$ and $[p53_p]$ exhibit two-phase dynamics; they first undergo three pulses and then switch to high

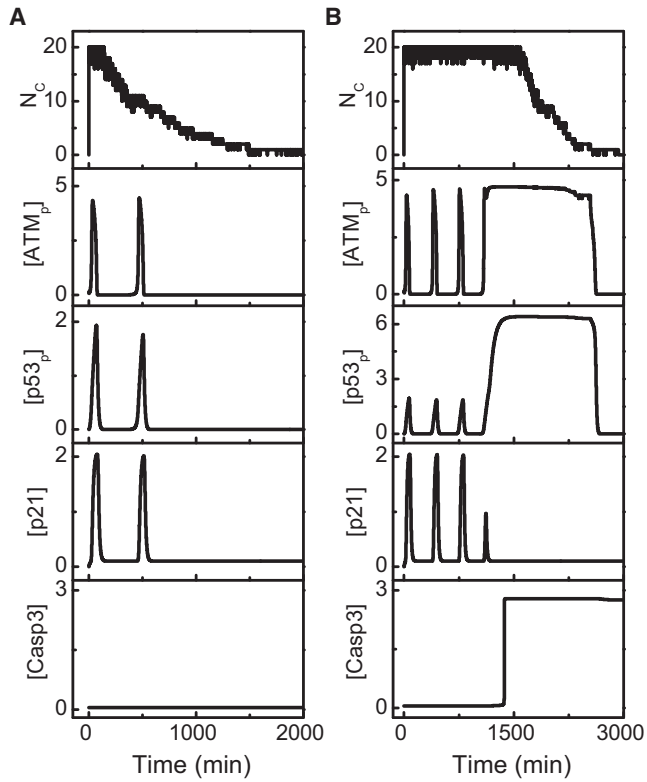

FIGURE 2 Dynamics of the p53 network. Time courses of (top to bottom) N_C, $[ATM_p]$, $[p53_p]$, [p21], and [Casp3] at $D_{IR} = 2$ Gy (*A*) or 6 Gy (*B*).

plateau levels. Accordingly, p53-arrester and p53-killer are the predominant forms of $p53_p$ in the first and second phases, respectively (Fig. S1). That is, p53 is first primarily activated and then fully activated. p21 is induced in the first phase, whereas Casp3 is activated in the second phase. Here, the irreversible activation of Casp3 is taken as a marker of apoptosis induction, and the downstream apoptotic events are not represented in the model. Thus, $[p53_p]$ still returns to basal levels after the damage is fixed. In fact, the repair proteins will be cleaved by Casp3, and the repair process will stop after Casp3 activation. Consequently, apoptosis is triggered before the DNA damage can be fully fixed in severely damaged cells. Taken together, the cell fate is closely associated with the network dynamics.

The two-phase behavior can be interpreted as follows. In the first phase, Wip1 is induced by p53-arrester (Fig. S1), and the ATM-p53-Wip1 negative feedback loop is essential for generating ATM and p53 pulses (14,35). In the second phase, Wip1 is expressed at low levels, and thus its repression of ATM_p is released, elevating both $[ATM_p]$ and $[p53_p]$. Moreover, PTEN is induced by p53-killer, and the p53-PTEN-Akt-Mdm2 positive feedback is markedly strengthened, leading to the sequestration of Mdm2 in the cytoplasm. Thus, $[p53_p]$ is driven to high levels. The above results are consistent with our previous report (14): the determination of cell fate is mediated by pulsing of p53 levels, and high levels of $p53_p$ facilitate apoptosis induction. Compared with the case with a deficiency in both miR-605 and miR-34a, however, here the percentage of apoptotic cells within a population can rise remarkably, and the average time required for Casp3 activation drops markedly at moderate doses, as shown later.

Influence of miR-605 on p53 activity

It was reported in our previous work that a sufficient amount of Wip1 is required for ATM and p53 oscillations (14). This conclusion holds true even when the p53-miR-605-Mdm2 positive feedback loop is included in the model. Fig. 3 *A* shows the bifurcation diagram of $[ATM_p]$ as a function of the p53-inducible synthesis rate of Wip1, k_{swip1}. Only when $k_{swip1} > 0.052$ can $[ATM_p]$ undergo oscillations; otherwise, $[ATM_p]$ shows bistability or monostability. There exists a minor difference in the upper and lower thresholds of k_{swip1} for bistability between the cases with $k_{smiR605} = 0$ and $k_{smiR605} = 0.02$ (the default value). In the following, we describe the difference in network dynamics between the two cases.

At $D_{IR} = 6$ Gy, [miR-605] also undergoes two phases in the case of $k_{smiR605} = 0.02$, because it is directly induced by $p53_p$, in contrast to a lower constant level in the case of $k_{smiR605} = 0$ (Fig. 3 *B*). The amplitude of $p53_p$ oscillation only changes slightly between the two cases (Fig. 3, *C* and *D*) (the difference will be enlarged with further increase of $k_{smiR605}$). However, a small change may be amplified via

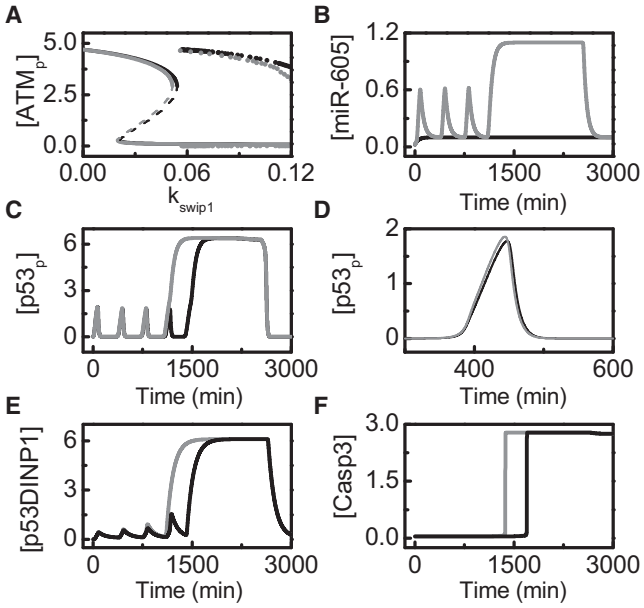

FIGURE 3 Network dynamics in the two cases with $k_{smir605} = 0$ (*black curves*) or 0.02 (*gray curves*). (*A*) Bifurcation diagram of $[ATM_p]$ versus k_{swip1}. N_C is kept at 20. The solid and dashed lines represent stable and unstable steady states, respectively. The dots represent the maximum and minimum of oscillations. (*B–F*) Time courses of the levels of miR-605 (*B*), $p53_p$ (*C* and *D*), p53DINP1 (*E*), and Casp3 (*F*) at $D_{IR} = 6$ Gy. The time course in *D* is a magnification of the second peak in *C*.

positive feedback, cascade responses, or temporal accumulation to elicit a large physiological effect. Indeed, the full activation of p53 and apoptosis are accelerated with $k_{smiR605} = 0.02$, as explained below.

As mentioned above, p53-induced p53DINP1 promotes the accumulation of p53-killer. Its concentration also oscillates in the early phase, but the amplitude rises gradually (Fig. 3 *E*). When [p53DINP1] reaches some threshold level, p53-killer begins to predominate over p53-arrester. The difference in [p53DINP1] between the two cases increases over time, and the threshold is reached first with $k_{smiR605} = 0.02$. Thus, the number of p53 pulses decreases by one, and Casp3 is activated 325 min earlier with $k_{smiR605} = 0.02$ than with $k_{smiR605} = 0$ (Fig. 3 *F*). Furthermore, it is shown in Fig. S2 that the histogram of the time required for Casp3 activation is centered at 1370 min with $k_{smiR605} = 0.02$, whereas it is centered around 1700 min with $k_{smiR605} = 0$. Taken together, miR-605 promotes the accumulation of fully activated p53 and facilitates p53-induced apoptosis. The effect of miR-605 on p53 dynamics could be tested experimentally by comparing the timing of p53 phosphorylation on Ser-46 in different situations. At high doses, overexpression of miR-605 would advance the accumulation of p53-killer, whereas knockdown of miR-605 would do the opposite.

Indeed, miR-605 functions by repressing the translation of *mdm2* mRNA to modulate p53 dynamics (9). At $D_{IR} = 2$ Gy, most of Mdm2 molecules enter the nucleus, and

thus [Mdm2$_n$] is much greater than [Mdm2$_c$] (Fig. 4, *A* and *B*). Both [Mdm2$_n$] and [Mdm2$_c$] are less at $k_{smiR605} = 0.02$ than at $k_{smiR605} = 0$. This difference is more remarkable during the second phase at $D_{IR} = 6$ Gy, especially for [Mdm2$_c$] (Fig. 4, *C* and *D*). The maximum of [Mdm2$_c$] in the case of $k_{smiR605} = 0.02$ is nearly half that in the case of $k_{smiR605} = 0$. This enhanced inhibition of [Mdm2$_c$] by miR-605 results from a marked increase in [miR-605] in the second phase. Thus, the downregulation of Mdm2 can be amplified by the p53-miR-605-Mdm2 loop. Of note, the remarkable reduction in [Mdm2$_c$] does not lead to a marked increase in [p53$_p$], since only a small amount of Mdm2 enters the nucleus due to PTEN induction.

Effects of miR-605 and PTEN on apoptosis induction

It has been reported that the expression of PTEN is important for high levels of p53 and apoptosis induction after severe DNA damage (14). At $k_{smiR605} = 0.02$, miR-605 shows no effect on the upregulation of p53 in the second phase, given PTEN induction (cf. Fig. 3 *C*). However, PTEN is often deficient in some cells, for example, because of its promoter methylation (44). This raises the issue of how [p53$_p$] would reach high levels to trigger apoptosis in that situation. We found that miR-605 may play a key role in promoting apoptosis, compensating for PTEN deficiency.

Since [p53$_p$], or [p53-killer] in the second phase, is close to the steady-state level of p53$_p$ at fixed $N_C = 20$ (ignoring DNA repair), we use the steady-state analysis to get an overall picture of how the expression of miR-605 affects [p53$_p$] in the second phase. With PTEN deficiency ($k_{sPTEN} = 0$), the steady-state level of p53$_p$ rises monotonically with increasing $k_{smiR605}$ (Fig. 5 *A*). That is, enhancing the expression of miR-605 elevates p53$_p$ levels. Fig. 5 *B* further shows the temporal evolution of [p53-killer] at $D_{IR} = 6$ Gy. After the initial few pulses with very low amplitudes, [p53-killer] can rise quickly to saturation. The time of onset, changing rate, and plateau level of [p53-killer] all vary gradually with $k_{smiR605}$. With $k_{smiR605} = 0.02$, [p53-killer] is not high enough, and thus Casp3 remains inactive. When $k_{smiR605} > 0.06$, Casp3 can be activated in a switchlike manner.

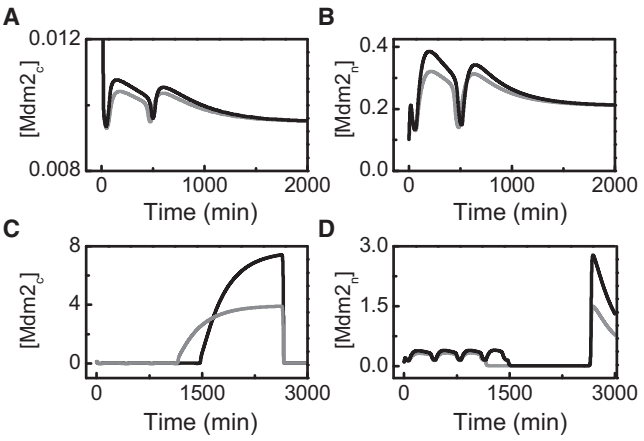

FIGURE 4 Effect of miR-605 on *mdm2* expression. Time courses of the levels of Mdm2$_c$ and Mdm2$_n$ at $D_{IR} = 2$ Gy (*A* and *B*) or 6 Gy (*C* and *D*). The gray and black curves correspond to $k_{smiR605} = 0.02$ and 0, respectively.

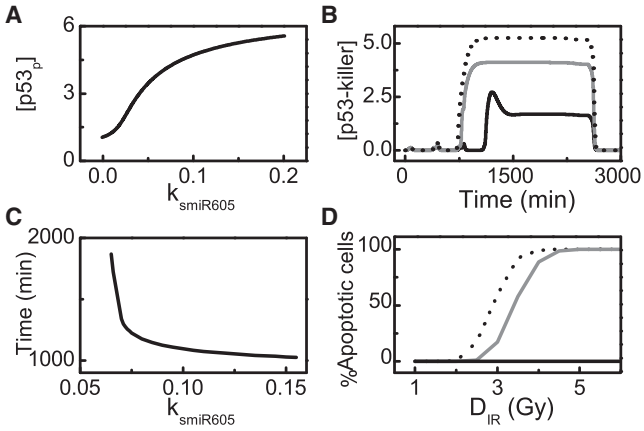

FIGURE 5 Effect of miR-605 on p53 activity and cellular outcome in the case of PTEN deficiency (with $k_{sPTEN} = 0$). (*A*) Bifurcation diagram of [p53$_p$] versus $k_{smiR605}$ at fixed $N_C = 20$. (*B*) Time courses of [p53-killer] at $D_{IR} = 6$ Gy with $k_{smiR605} = 0.02$ (*black*), 0.07 (*gray*), or 0.15 (*dotted*). (*C*) Mean time required to activate Casp3 at $D_{IR} = 6$ Gy as a function of $k_{smiR605}$. (*D*) Percentage of apoptosis among a population of 2000 cells versus D_{IR} with $k_{smiR605} = 0.02$ (*black*), 0.07 (*gray*), or 0.15 (*dotted*).

In a population of cells exposed to the same irradiation, different numbers of DSBs can be induced in each cell, obeying a Poisson distribution, and thus there may exist distinct cellular outcomes. As seen in Fig. 5 *C*, the mean time required to activate Casp3 drops with increasing $k_{smiR605}$. Fig. 5 *D* shows the percentage of apoptotic cells as function of the radiation dose, D_{IR}, for different values of $k_{smiR605}$. The percentage rises gradually toward 100% with increasing D_{IR} at fixed $k_{smiR605}$ (>0.06); it also rises with increasing $k_{smiR605}$ if $D_{IR} < 4.5$ Gy. That is, enhancing the expression of miR-605 contributes to p53-dependent apoptosis in PTEN-deficient cells. Thus, upregulation of p53 to induce apoptosis occurs by two mechanisms, repressing the expression of *mdm2* by miR-605 and sequestering Mdm2 in the cytoplasm through PTEN.

It is worth noting that the network dynamics is influenced differently by PTEN than by miR-605. With $k_{smiR605} = 0.02$, the steady-state level of p53$_p$ can exhibit bistability over a range of k_{sPTEN} (0.13–0.26) (Fig. 6 *A*). Beyond that region, [p53$_p$] settles at a moderate or high level. With $k_{sPTEN} = 0$, p53-killer predominates over p53-arrester after three pulses at $D_{IR} = 6$ Gy (Fig. 6 *B*), but its level is not high enough, and Casp3 remains inactive (Fig. 6 *C*). With $k_{sPTEN} = 0.14$ or 0.5 (the default value), [p53-killer] is maintained at relatively high levels in the second phase, and thus Casp3 is activated to induce apoptosis. Interestingly, the timing of Casp3 activation changes slightly with k_{sPTEN}.

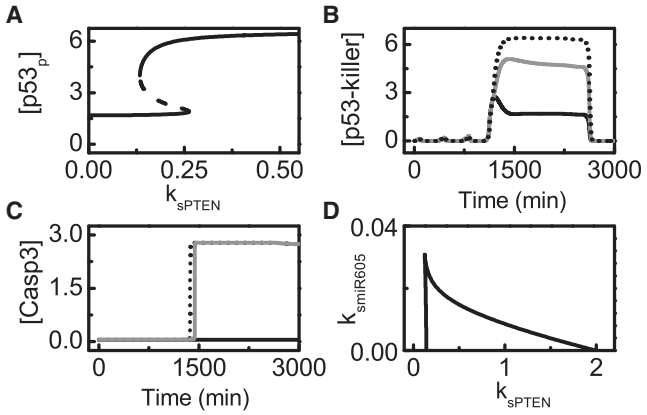

FIGURE 6 Effect of PTEN on p53 activity and cellular outcome. (*A*) Bifurcation diagram of [p53$_p$] versus k_{sPTEN} at fixed $N_C = 20$. The stable and unstable steady states are denoted by solid and dashed lines, respectively. (*B* and *C*) Time courses of [p53-killer] (*B*) and [Casp3] (*C*) at $D_{IR} = 6$ Gy with $k_{sPTEN} = 0$ (*black*), 0.14 (*gray*), or 0.5 (*dotted*). $k_{smiR605} = 0.02$ in *A*–*C*. (*D*) To explore how the bifurcation points in Fig. 6 *A* change with varying $k_{smiR605}$, Fig. 6 *D* shows the dependence of the upper and lower thresholds of k_{sPTEN} on $k_{smiR605}$.

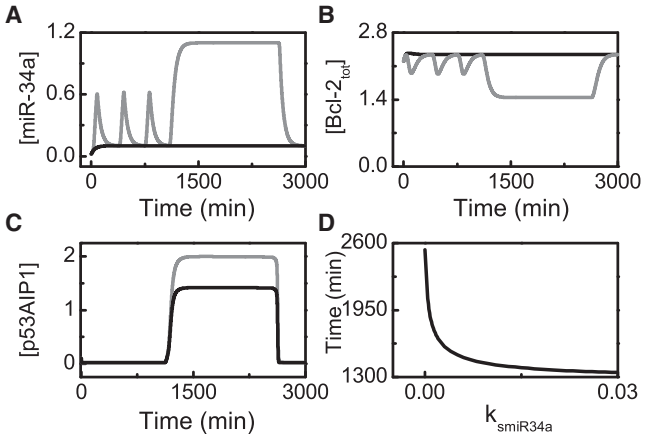

FIGURE 7 Effect of miR-34a on Bcl-2 activity and cellular outcome at $D_{IR} = 6$ Gy. Time courses of [miR-34a] (*A*), [Bcl-2$_{tot}$] (*B*), and [p53AIP1] (*C*). The gray and black curves correspond to the cases with $k_{smiR34a} = 0.02$ and 0, respectively. (*D*) Mean time required to activate Casp3, averaged over 2000 cells, versus $k_{smiR34a}$.

Taken together, these findings suggest that a sufficient amount of PTEN is required to induce apoptosis in severely damaged cells; otherwise, enough miR-605 is required. In fact, the two can complement each other in apoptosis induction (see below).

The two-parameter bifurcation diagram of $k_{smiR605}$ versus k_{sPTEN} characterizes the dependence of the upper and lower thresholds of k_{sPTEN} on $k_{smiR605}$ (Fig. 6 *D*). The lower threshold of k_{sPTEN} nearly remains fixed, whereas the upper threshold drops with increasing $k_{smiR605}$. To ensure apoptosis induction after severe DNA damage, the values of k_{sPTEN} and $k_{smiR605}$ should be taken from the top right region beyond that enclosed by two threshold lines. It should be noted that sufficient expression of miR-605 or PTEN is required when the other is deficient. miR-605 and PTEN are separately involved in p53-centered positive feedback loops, elevating p53$_p$ levels by downregulating nuclear Mdm2. However, PTEN is induced in the later phase of the cellular response to severe damage, whereas miR-605 has a role during the whole cellular response. Distinguishing the difference between miR-605 and PTEN may be important for designing efficient cancer therapies.

Effect of miR-34a on apoptosis induction

In our model, miR-34a represses the translation of *bcl-2* mRNA, increasing the amount of free p53AIP1. We first compare the network dynamics when the p53-inducible synthesis rate of miR-34a, $k_{smiR34a}$, is 0 or 0.02. With $k_{smiR34a} = 0.02$, the level of miR-34a also undergoes two-phase dynamics at $D_{IR} = 6$ Gy, since it is directly induced by p53$_p$ (Fig. 7 *A*). [miR-34a] reaches a relatively high level in the second phase, promoting apoptosis induction. [Bcl-2$_{tot}$] is reversely correlated with [miR-34a] (Fig. 7 *B*; see also Fig. S3); [Bcl-2$_{tot}$] drops markedly to an intermediate level in the second phase, and the concentration of free p53AIP1 is maintained at a relatively high level (Fig. 7 *C*). In contrast, with $k_{smiR34a} = 0$, [miR-34a] remains at a rather low level, whereas [Bcl-2$_{tot}$] is kept at a high level; accordingly, [p53AIP1] settles at an intermediate level. Note that the mean time required to activate Casp3 rises remarkably with decreasing $k_{smiR34a}$ (Fig. 7 *D*). When $k_{smiR34a}$ drops from 0.02 to 0, for example, Casp3 activation is delayed by ~1165 min. This marked delay results from the extended integration of [Casp3] to reach its threshold level for activation (Fig. S3). Therefore, enhancing the expression of miR-34a contributes to timely removal of irreparably damaged cells. Compared with miR-605, miR-34a is more directly involved in apoptosis induction.

It is interesting to compare the timing of Casp3 activation at $D_{IR} = 6$ Gy under four conditions (Fig. 8 *A*). The curves from left to right correspond to the cases with normal expression of both miR-34 and miR-605, miR-34a alone, miR-605 alone, and with a deficiency in both miR-605 and miR-34a, respectively. Remarkably, apoptosis is accelerated to an extent that depends on the expression of miRNAs. The curves of the percentage of apoptotic cells versus D_{IR} (Fig. 8 *B*) shift to the right in the same order as in Fig. 8 *A*. With the default parameter setting, more apoptosis can be induced with $k_{smiR34a} = 0.02$ and $k_{smiR605} = 0$ than with $k_{smiR605} = 0.02$ and $k_{smiR34a} = 0$ for $3 < D_{IR} < 8$ Gy. We note that our simulation results agree with the quantified experimental data from Fig. 5 of Xiao et al. (9) (Fig. 8 *C*, *left* and *right*, respectively).

To explain these differences, we show the temporal evolution of [p53$_p$] and [Casp3] at $D_{IR} = 5$ Gy under various conditions (Fig. S4). Only when [p53DINP1] reaches some threshold does p53-killer become dominant over

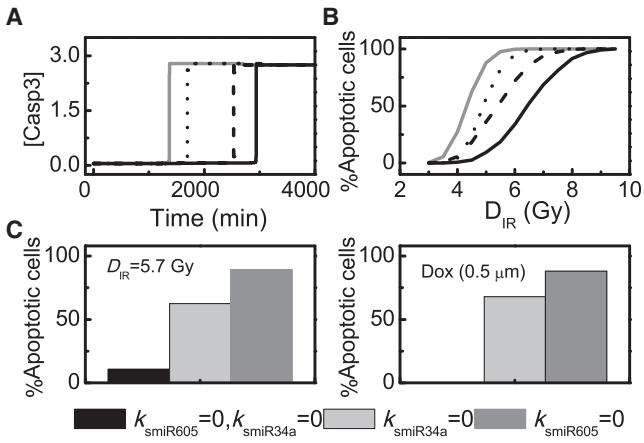

FIGURE 8 Effect of miR-34a and miR-605 on apoptosis induction. (*A*) Time courses of [Casp3] at $D_{IR} = 6$ Gy. (*B*) Percentage of apoptotic cells within a population of 2000 cells versus D_{IR}. Four cases are compared with $k_{smiR605} = 0.02$ and $k_{smiR34a} = 0.02$ (*gray*), $k_{smiR605} = 0$ and $k_{smiR34a} = 0.02$ (*dotted*), $k_{smiR605} = 0.02$ and $k_{smiR34a} = 0$ (*dashed*), and $k_{smiR605} = 0$ and $k_{smiR34a} = 0$ (*black*). (*C*) Percentage of apoptotic cells from our simulations (*left*) and from the experimental data (*right*).

p53-arrester, which is a prerequisite for apoptosis induction. miR-605 accelerates the accumulation of p53DINP1, which makes it possible for some cells to commit apoptosis at moderate levels of DNA damage. Without enough miR-605, the DNA damage might be fixed before [p53DINP1] can reach the threshold, or it could take longer for [p53-killer] to accumulate remarkably. On the other hand, enough accumulation of free p53AIP1 is required to induce CytoC release and Casp3 activation. miR-34a contributes to this process of accumulation: without enough miR-34a, Casp3 may remain inactive even though [$p53_p$] is driven to high levels, or it may take longer to activate Casp3. Collectively, both miR-34a and miR-605 can promote apoptosis induction; miR-34a acts directly, while miR-605 acts indirectly through enhancing p53 activation. It would be interesting to experimentally justify the above conclusion. With overexpression or knockdown of either miRNA and their different combinations, the temporal evolution of p53AIP1 and Casp3 levels is monitored so as to reveal different effects of miR-605 and miR-34a on cellular outcome. This may advance the understanding of how miRNAs acting upstream or downstream of p53 regulate its tumor suppressor function.

DISCUSSION

p53 can regulate gene transcription as well as processing and maturation of target miRNAs, and the list of p53-targeted miRNAs grows increasingly longer (11). Several p53-targeted miRNAs can modulate p53 activity markedly. miR-605 is the first miRNA identified as upregulating p53 by repressing the translation of *mdm2* mRNA (9). Very recently, it was reported that miR-143 and miR-145, induced by p53, also enhance p53 activation by suppressing the translation of *mdm2* mRNA (16). On the other hand, p53-induced miR-16 promotes apoptosis by suppressing the expression of *bcl-2* (45), in a way similar to that observed for miR-34a. For simplicity, here we chose only miR-605 and miR-34a as two representatives of p53-targeted miRNAs, which function upstream and downstream, respectively, of p53. It would be intriguing to extend this model to test whether the main conclusions drawn here hold true when more proapoptotic miRNAs are added to the p53 network.

It is noteworthy that miR-34a also enhances p53 acetylation by inhibiting the SIRT1 deacetylase posttranscriptionally in HCT116 cells (46). However, miR-34a acts only downstream of p53 in MCF-7 cells, where knockdown of miR-34a does not alter the transcriptional activity of p53 (9). Thus, the function of miR-34a in the p53 network may be specific to cell type. Here, we aimed to model non-transformed MCF-10A cells in which the action mode of miR-34a is similar to that seen in MCF-7 cells. In our work, miR-605 accelerates the full activation of p53 by suppressing Mdm2, while miR-34a facilitates p53-dependent apoptosis by repressing Bcl-2. Together, miR-605 and miR-34a can enhance the tumor suppressor function of p53 in various ways.

Our simulation results indicate that both miR-605 and PTEN can elevate p53 levels by downregulating nuclear Mdm2. miR-605 represses the translation of *mdm2* mRNA, while PTEN inhibits entry of Mdm2 into the nucleus. They can complement each other in the upregulation of p53 to evoke apoptosis. This may have important implications for cancer therapy. In PTEN-deficient cell lines such as MCF-7 cells, for example, enhancing the expression of miR-605 would contribute to full activation of p53 after severe DNA damage. Alternatively, PTEN is required for p53-dependent apoptosis in miR-605-deficient cell lines such as A549 cells (9).

Our model predicts that both miR-605 and miR-34a affect whether a cell commits to apoptosis and the timing of apoptosis initiation. In the model, p53DINP1 should accumulate enough to induce the conversion from p53-arrester to p53-killer, and the amount of free p53AIP1 should be high enough to activate CytoC release and Casp3 activation. miR-605 and miR-34a contribute separately to these two processes. Such a dual control mechanism for apoptosis induction adds another level of complexity to regulation of cellular output. Moreover, miR-605 can promote the expression of *p53AIP1* to increase the total amount of p53AIP1 via p53, which also facilitates apoptosis induction. Therefore, miR-605 and miR-34a together endow the network with a fail-safe mechanism for apoptosis induction.

The finding that miR-605 and miR-34a have such a marked effect on the cell-fate decision and timing of apoptosis is unexpected, given that they only modulate translation of mRNAs. As seen in Fig. 3, whereas the

amplitude of p53 oscillation changes slightly due to miR-605 regulation, the activation of Casp3 can be advanced remarkably. In a similar way, miR-34a contributes markedly to apoptosis induction (Fig. 7 *D*). The coordination between miR-605 and miR-34a also plays a key role in cell-fate control (Fig. 8). Obviously, without constructing an integrated network model of the p53 pathway and a detailed analysis of network dynamics, it was not possible to reveal here the remarkable contribution of miR-605 and miR-34a to p53-dependent apoptosis, even though we know their connection with p53. This work suggests that the influence of miRNAs on cellular signaling may be amplified via feedback and feed-forward loops, and it sheds light on the action modes of miRNAs.

It should be noted that miR-605 and miR-34a affect the cell fate and timing of apoptosis largely because they are important nodes of the p53 pathway and their effect on gene expression is amplified. miR-605 can upregulate p53, modulating the conversion of p53-arrester to p53-killer, while miR-34a affects the level of free p53AIP1, thereby mediating initiation of the caspase cascade. In our model, the kinetics of miRNA induction are determined by p53 and do not play a critical role in cellular outcome. Nevertheless, it is worthwhile to systematically explore what roles the dynamics of miRNA expression may have in a larger p53 network that includes more miRNA species. Moreover, we previously showed that the action mode of p53 (pulsing or switching) in the second phase also markedly modulates the timing of apoptosis (14). It would be interesting to compare the contribution of these different mechanisms to cell-fate control.

CONCLUSION

In this study, we developed a four-module network model to probe the roles of two p53-targeted miRNAs, miR-605 and miR-34a, in the modulation of p53 dynamics and DDR. Whereas single miRNAs may have a minor effect on protein levels, their combined effects may be amplified via various mechanisms. Our results indicate that miR-605 can elevate p53 levels and promote its full activation, while miR-34a directly promotes apoptosis by inhibiting the antiapoptotic factors. Given the protein-miRNA interactions in the p53 network, the previously proposed mechanism for cell-fate decision by p53 pulses still holds true. With the proapoptotic miRNAs joining the p53 network, apoptosis can be accelerated to remove irreparably damaged cells promptly. Therefore, taking into account the role of miRNAs in p53 signaling may provide new clues to p53-dependent cancer treatments.

SUPPORTING MATERIAL

Two tables, four figures, Supporting Methods, model equations, and references (47,48) are available at http://www.biophysj.org/biophysj/supplemental/S0006-3495(14)00278-1.

The authors declare that no competing interests exist.

This work was supported by the 973 program (No. 2013CB834104), National Natural Science Foundation of China (Nos. 11175084, 81121062, and 11204126), and the Priority Academic Program Development of Jiangsu Higher Education Institutions.

REFERENCES

1. Filipowicz, W., S. N. Bhattacharyya, and N. Sonenberg. 2008. Mechanisms of post-transcriptional regulation by microRNAs: are the answers in sight? *Nat. Rev. Genet.* 9:102–114.
2. Lewis, B. P., C. B. Burge, and D. P. Bartel. 2005. Conserved seed pairing, often flanked by adenosines, indicates that thousands of human genes are microRNA targets. *Cell.* 120:15–20.
3. Ebert, M. S., and P. A. Sharp. 2012. Roles for microRNAs in conferring robustness to biological processes. *Cell.* 149:515–524.
4. Vousden, K. H., and D. P. Lane. 2007. p53 in health and disease. *Nat. Rev. Mol. Cell Biol.* 8:275–283.
5. Vousden, K. H. 2006. Outcomes of p53 activation—spoilt for choice. *J. Cell Sci.* 119:5015–5020.
6. He, L., X. He, …, G. J. Hannon. 2007. A microRNA component of the p53 tumour suppressor network. *Nature.* 447:1130–1134.
7. Pichiorri, F., S. S. Suh, …, C. M. Croce. 2010. Downregulation of p53-inducible microRNAs 192, 194, and 215 impairs the p53/MDM2 autoregulatory loop in multiple myeloma development. *Cancer Cell.* 18:367–381.
8. Yamakuchi, M., C. D. Lotterman, …, C. J. Lowenstein. 2010. P53-induced microRNA-107 inhibits HIF-1 and tumor angiogenesis. *Proc. Natl. Acad. Sci. USA.* 107:6334–6339.
9. Xiao, J., H. Lin, …, Z. Wang. 2011. miR-605 joins p53 network to form a p53:miR-605:Mdm2 positive feedback loop in response to stress. *EMBO J.* 30:524–532.
10. Suzuki, H. I., K. Yamagata, …, K. Miyazono. 2009. Modulation of microRNA processing by p53. *Nature.* 460:529–533.
11. Feng, Z., C. Zhang, …, W. Hu. 2011. Tumor suppressor p53 meets microRNAs. *J. Mol. Cell Biol.* 3:44–50.
12. Purvis, J. E., K. W. Karhohs, …, G. Lahav. 2012. p53 dynamics control cell fate. *Science.* 336:1440–1444.
13. Zhang, X. P., F. Liu, …, W. Wang. 2009. Cell fate decision mediated by p53 pulses. *Proc. Natl. Acad. Sci. USA.* 106:12245–12250.
14. Zhang, X. P., F. Liu, and W. Wang. 2011. Two-phase dynamics of p53 in the DNA damage response. *Proc. Natl. Acad. Sci. USA.* 108:8990–8995.
15. Choi, M., J. Shi, …, K. H. Cho. 2012. Attractor landscape analysis reveals feedback loops in the p53 network that control the cellular response to DNA damage. *Sci. Signal.* 5:ra83.
16. Zhang, J., Q. Sun, …, W. T. Chen. 2013. Loss of microRNA-143/145 disturbs cellular growth and apoptosis of human epithelial cancers by impairing the MDM2-p53 feedback loop. *Oncogene.* 32:61–69.
17. Zhang, X., G. Wan, …, X. Lu. 2010. Oncogenic Wip1 phosphatase is inhibited by miR-16 in the DNA damage signaling pathway. *Cancer Res.* 70:7176–7186.
18. Chang, T. C., E. A. Wentzel, …, J. T. Mendell. 2007. Transactivation of miR-34a by p53 broadly influences gene expression and promotes apoptosis. *Mol. Cell.* 26:745–752.
19. Raver-Shapira, N., E. Marciano, …, M. Oren. 2007. Transcriptional activation of miR-34a contributes to p53-mediated apoptosis. *Mol. Cell.* 26:731–743.
20. Hermeking, H. 2010. The miR-34 family in cancer and apoptosis. *Cell Death Differ.* 17:193–199.
21. Hermeking, H. 2012. MicroRNAs in the p53 network: micromanagement of tumour suppression. *Nat. Rev. Cancer.* 12:613–626.

22. Harris, S. L., and A. J. Levine. 2005. The p53 pathway: positive and negative feedback loops. *Oncogene.* 24:2899–2908.

23. Rothkamm, K., I. Krüger, …, M. Löbrich. 2003. Pathways of DNA double-strand break repair during the mammalian cell cycle. *Mol. Cell. Biol.* 23:5706–5715.

24. Ma, L., J. Wagner, …, G. A. Stolovitzky. 2005. A plausible model for the digital response of p53 to DNA damage. *Proc. Natl. Acad. Sci. USA.* 102:14266–14271.

25. Stewart, R. D. 2001. Two-lesion kinetic model of double-strand break rejoining and cell killing. *Radiat. Res.* 156:365–378.

26. Bakkenist, C. J., and M. B. Kastan. 2003. DNA damage activates ATM through intermolecular autophosphorylation and dimer dissociation. *Nature.* 421:499–506.

27. Stommel, J. M., and G. M. Wahl. 2004. Accelerated MDM2 auto-degradation induced by DNA-damage kinases is required for p53 activation. *EMBO J.* 23:1547–1556.

28. Prives, C. 1998. Signaling to p53: breaking the MDM2-p53 circuit. *Cell.* 95:5–8.

29. Oda, K., H. Arakawa, …, Y. Taya. 2000. p53AIP1, a potential mediator of p53-dependent apoptosis, and its regulation by Ser-46-phosphorylated p53. *Cell.* 102:849–862.

30. Okamura, S., H. Arakawa, …, Y. Nakamura. 2001. p53DINP1, a p53-inducible gene, regulates p53-dependent apoptosis. *Mol. Cell.* 8:85–94.

31. Mayo, L. D., and D. B. Donner. 2001. A phosphatidylinositol 3-kinase/Akt pathway promotes translocation of Mdm2 from the cytoplasm to the nucleus. *Proc. Natl. Acad. Sci. USA.* 98:11598–11603.

32. Mayo, L. D., Y. R. Seo, …, D. B. Donner. 2005. Phosphorylation of human p53 at serine 46 determines promoter selection and whether apoptosis is attenuated or amplified. *J. Biol. Chem.* 280:25953–25959.

33. Takekawa, M., M. Adachi, …, K. Imai. 2000. p53-inducible wip1 phosphatase mediates a negative feedback regulation of p38 MAPK-p53 signaling in response to UV radiation. *EMBO J.* 19:6517–6526.

34. Shreeram, S., O. N. Demidov, …, D. V. Bulavin. 2006. Wip1 phosphatase modulates ATM-dependent signaling pathways. *Mol. Cell.* 23: 757–764.

35. Batchelor, E., C. S. Mock, …, G. Lahav. 2008. Recurrent initiation: a mechanism for triggering p53 pulses in response to DNA damage. *Mol. Cell.* 30:277–289.

36. Stambolic, V., A. Suzuki, …, T. W. Mak. 1998. Negative regulation of PKB/Akt-dependent cell survival by the tumor suppressor PTEN. *Cell.* 95:29–39.

37. Manning, B. D., and L. C. Cantley. 2007. AKT/PKB signaling: navigating downstream. *Cell.* 129:1261–1274.

38. Trotman, L. C., and P. P. Pandolfi. 2003. PTEN and p53: who will get the upper hand? *Cancer Cell.* 3:97–99.

39. Matsuda, K., K. Yoshida, …, H. Arakawa. 2002. p53AIP1 regulates the mitochondrial apoptotic pathway. *Cancer Res.* 62:2883–2889.

40. Ow, Y. P., D. R. Green, …, T. W. Mak. 2008. Cytochrome *c*: functions beyond respiration. *Nat. Rev. Mol. Cell Biol.* 9:532–542.

41. Kirsch, D. G., A. Doseff, …, J. M. Hardwick. 1999. Caspase-3-dependent cleavage of Bcl-2 promotes release of cytochrome *c*. *J. Biol. Chem.* 274:21155–21161.

42. Riedl, S. J., and G. S. Salvesen. 2007. The apoptosome: signalling platform of cell death. *Nat. Rev. Mol. Cell Biol.* 8:405–413.

43. Jeffrey, P. D., S. Gorina, and N. P. Pavletich. 1995. Crystal structure of the tetramerization domain of the p53 tumor suppressor at 1.7 Å. *Science.* 267:1498–1502.

44. García, J. M., J. Silva, …, F. Bonilla. 2004. Promoter methylation of the PTEN gene is a common molecular change in breast cancer. *Genes Chromosomes Cancer.* 41:117–124.

45. Cimmino, A., G. A. Calin, …, C. M. Croce. 2005. miR-15 and miR-16 induce apoptosis by targeting BCL2. *Proc. Natl. Acad. Sci. USA.* 102:13944–13949.

46. Yamakuchi, M., M. Ferlito, and C. J. Lowenstein. 2008. miR-34a repression of SIRT1 regulates apoptosis. *Proc. Natl. Acad. Sci. USA.* 105:13421–13426.

47. Lavin, M. F., and N. Gueven. 2006. The complexity of p53 stabilization and activation. *Cell Death Differ.* 13:941–950.

48. Gottlieb, T. M., J. F. Leal, …, M. Oren. 2002. Cross-talk between Akt, p53 and Mdm2: possible implications for the regulation of apoptosis. *Oncogene.* 21:1299–1303.

Supporting Material

Involvement of miR-605 and miR-34a in the DNA Damage Response Promotes Apoptosis Induction

Chun-Hong Zhou, Xiao-Peng Zhang, Feng Liu, and Wei Wang

In this work, we mainly explored the effects of two p53-targeted miRNAs, miR-605 and miR-34a, on p53 dynamics and cellular outcome following DNA damage induced by ionizing radiation (IR). miR-605 and miR-34a separately repress the translation of *mdm2* and *bcl-2* mRNAs [1, 2], enhancing the tumor suppression function of p53. We proposed a four-module network model of the p53 signaling pathway. The model characterizes the DNA repair, ATM activation, regulation of p53 activity, and determination of cell output. This document includes the details of model construction (together with ordinary differential equations), two tables, and four figures.

Supplemental Method: Model construction

DNA repair. Double-strand breaks (DSBs) are the principal form of DNA damage caused by IR. In mammalian cells, DSBs are fixed through HR (homologous recombination) and NHEJ (nonhomologous end joining) [3]. Since HR requires a sister chromatid as a template, it mainly contributes to DSB repair in S/G2 phases. NHEJ simply associates two broken ends together and is the predominant repair pathway, especially active in the G1 phase. Here, we refer to the NHEJ pathway.

A two-lesion kinetic (TLK) model has been proposed to describe the repair process [4]. Of note, simple DSBs can be fixed quickly, whereas complex DSBs are fixed rather slowly. Given the stochasticity in the generation and repair of DSBs, we use the Monte Carlo method to simulate the repair process [5]. The irradiation dose is denoted by y Gy. The expected total number of DSBs in each cell obeys a Poisson distribution with a mean of $35y$, and the total number of repair proteins is assumed to be 20 per cell. Each damage site may be in one of three states, corresponding to intact DSB (D state), DSB in complex with repair protein (C state), and fixed DSB (F state). The numbers of damage sites in each state are denoted by N_{D}, N_{C}, and N_{F}, respectively. We use subscripts '1' and '2' to differentiate fast kinetics from slow kinetics. The Monte Carlo algorithm for the repair dynamics is based on

the transition probabilities between two neighboring states as follows [6]:

$$\begin{aligned}
P_{D_1\to C_1} &= N_{RP}[k_{fb1} + k_{cross}(N_{D1} + N_{D2})]\Delta t \\
P_{D_2\to C_2} &= N_{RP}[k_{fb2} + k_{cross}(N_{D1} + N_{D2})]\Delta t \\
P_{C_1\to D_1} &= k_{rb1}\Delta t \\
P_{C_2\to D_2} &= k_{rb2}\Delta t \\
P_{C_1\to F_1} &= k_{fix1}\Delta t \\
P_{C_2\to F_2} &= k_{fix2}\Delta t.
\end{aligned}$$

N_{RP} denotes the number of repair proteins. Δt represents the time step of integration, which is taken as 0.01 min in simulations. All of rate constants, k_{fb}, k_{cross}, k_{rb} and k_{fix}, are listed in *Supplemental Table* S2.

The Monte Carlo algorithm for the repair of DSBs caused by IR of y Gy during the time $[0, T_{\max}]$ is presented as follows [7]:

1. Initialization. Set $t = 0$. The total number of initial DSBs, $N_{\mathrm{D}}(0)$, is generated from a Poisson distribution with a mean of $35y$. The initial values for simple and complex DSB repair are taken as $N_{\mathrm{D1}}(0) = 0.7N_{\mathrm{D}}(0)$ and $N_{\mathrm{D2}}(0) = 0.3N_{\mathrm{D}}(0)$, while $N_{\mathrm{C1}}(0) = N_{\mathrm{C2}}(0) = N_{\mathrm{F1}}(0) = N_{\mathrm{F2}}(0) = 0$. The total number of repair proteins is set to 20, and the number of free repair proteins is $N_{\mathrm{RP}}(0) = 20$.

2. Increment time. Set $t = t + \Delta t$.

3. Update the state of each damage site controlled by fast repair. For each damage locus i (with $1 \le i \le N_{\mathrm{D1}}(0)$), a random number r is generated from a uniform distribution between 0 and 1. If the damage at locus i is in state D, a transition to state C occurs if $r < P_{D_1\to C_1}$, or it stays in state D. If the damage is in state C, a transition to state D occurs if $r < P_{C_1\to D_1}$, or a transition to state F occurs if $P_{C_1\to D_1} \le r < P_{C_1\to D_1}+P_{C_1\to F_1}$. If the damage is in state F, it always stays there (i.e., state F is absorbing). Set $N_{\mathrm{RP}} = N_{\mathrm{RP}} + 1$ if transition from state C to D or from state C to F occurs, or set $N_{\mathrm{RP}} = N_{\mathrm{RP}} - 1$ if transition from state D to C occurs; otherwise N_{RP} remains the same. After the last damage site has been updated, set the numbers of damage sites in states D, C, and F at time t to be N_{D1}, N_{C1} and N_{F1}, respectively.

4. Update the state of each damage site controlled by slow repair. For each damage locus i (with $1 \le i \le N_{\mathrm{D2}}(0)$), a random number r is produced from a uniform distribution

between 0 and 1. If the damage at locus i is in state D, a transition to state C occurs if $r < P_{D_2 \to C_2}$, or it stays in state D. If the damage is in state C, a transition to state D occurs if $r < P_{C_2 \to D_2}$, or a transition to state F occurs if $P_{C_2 \to D_2} \leq r < P_{C_2 \to D_2} + P_{C_2 \to F_2}$. If the damage is in state F, it always stays there. Set $N_{\mathrm{RP}} = N_{\mathrm{RP}} + 1$ if transition from state C to D or from state C to F occurs, or set $N_{\mathrm{RP}} = N_{\mathrm{RP}} - 1$ if transition from state D to C occurs; otherwise N_{RP} remains the same. After the last damage site has been updated, set the numbers of damage sites in states D, C, and F at time t to be N_{D2}, N_{C2} and N_{F2}, respectively.

5. Let $N_{\mathrm{D}}(t) = N_{\mathrm{D1}}(t) + N_{\mathrm{D2}}(t)$, $N_{\mathrm{C}}(t) = N_{\mathrm{C1}}(t) + N_{\mathrm{C2}}(t)$, and $N_{\mathrm{F}}(t) = N_{\mathrm{F1}}(t) + N_{\mathrm{F2}}(t)$.
6. Repeat steps 2-5 until all the DSBs are effectively repaired (i.e.,$N_{\mathrm{D}}(\mathrm{t}) + N_{\mathrm{C}}(t) \leq 2$).

ATM sensor. The ATM kinase detects the presence of DSBs. Upon IR, the inactive ATM dimer is disassociated into active, phosphorylated monomer through intermolecular phosphorylation [8]. Here, three forms of ATM are considered: $\mathrm{ATM_d}$ (inactive dimer), ATM (inactive monomer) and $\mathrm{ATM_p}$ (active monomer). The total concentration of ATM is assumed to be a constant ($\mathrm{ATM_{tot}}$) because ATM is regulated posttranslationally after IR [8]. Given ATM is activated by DSB repair-protein complexes (DSBCs), the rate of ATM activation depends on N_{C}. In addition, Wip1 promotes $\mathrm{ATM_p}$ inactivation through dephosphorylation [9]. The dynamics of this module are characterized by Eqs. 1-3. The phosphorylation and dephosphorylation processes are considered as enzyme-catalyzed reactions, and they are assumed to follow the Michaelis-Menten kinetics. The dimerization rate of ATM is much greater than its undimerization rate, so that ATM dimers are predominant in unstressed cells [5].

p53-centered feedback control. Activated ATM phosphorylates p53 and Mdm2, blocking the p53-Mdm2 interaction. We consider three forms of nuclear p53: un-phosphorylated (p53, inactive form), phosphorylated at Ser15 (p53-arrester, primarily activated form), and doubly phosphorylated at Ser15 and Ser46 (p53-killer, fully activated form) [6]. Phosphorylated p53 is collectively symbolized by $\mathrm{p53_p}$. Three forms of Mdm2 are considered: dephosphorylated cytoplasmic form ($\mathrm{Mdm2_c}$), phosphorylated cytoplasmic form ($\mathrm{Mdm2_{cp}}$), and nuclear form ($\mathrm{Mdm2_n}$). The mdm2 mRNA, mdm2m, is also included in the model.

There exist four p53-centered feedback loops: the p53-miR-605-Mdm2 and p53-PTEN-

Akt-Mdm2 positive feedback loops, as well as the p53-Mdm2 and ATM-p53-Wip1 negative feedback loops. The dynamics of this module are described by Eqs. 4-17. All the transcription of genes by p53 is characterized by Hill function, and the Hill efficient is set to 4 given the cooperativity of the tetrameric form of p53 as a transcription factor [10].

The production rate of p53 is assumed to be constant because p53 is mainly regulated by posttranslational modifications [11]. Since ATM-dependent phosphorylation of p53 and $\mathrm{Mdm2_n}$ can be considered as enzyme-catalytic reactions, both the activation rate of p53 and the degradation rate of $\mathrm{Mdm2_n}$ are assumed to depend on $\mathrm{ATM_p}$ level in a Michaelis-Menten form. p53 is targeted for proteasomal degradation by $\mathrm{Mdm2_n}$, which is characterized by the Michaelis-Menten dynamics. We set $k_{\mathrm{dp53p}} \ll k_{\mathrm{dp53}}$ because the weak binding affinity of $\mathrm{Mdm2_n}$ to $\mathrm{p53_p}$ prevents its degradation [5].

Moreover, it is assumed that $\mathrm{Akt_p}$ promotes the conversion from $\mathrm{Mdm2_c}$ to $\mathrm{Mdm2_{cp}}$ by phosphorylation and only $\mathrm{Mdm2_{cp}}$ can enter the nucleus to degrade p53 [12]. The total level of Akt is assumed to be constant since no significant changes were observed in the DNA damage response [13]. Similarly, the total level of PIP3 and PIP2 is also assumed to be constant.

p53-mediated cell fate decision. Based on the phosphorylation status, active p53 is divided into p53-arrester and p53-killer. p53-arrester transactivates *p21, Wip1*, and *p53DINAP1*, while p53-killer transactivates *PTEN, p53AIP1*, and *p53DINP1* [6]. p21 induces cell-cycle arrest, while p53AIP1 induces the release of cytochrome c, which activates caspase-3 to trigger apoptosis.

The dynamics of this module are described by Eqs. 18-31. The transition between p53-arrester and p53-killer is a key step for the selective expression of target genes by p53, depending on the levels of p53DINP1 and Wip1. The rate constant of p53DINP1 induction by p53-killer is much greater than that by p53-arrester since p53-killer has a higher affinity to the promoter of P53DINP1 than p53-arrester [14]. The expression of Bcl-2 is repressed by miR-34a, and the expression rate is assumed to obey the Michaelis-Menten dynamics for simplicity. The association rate between Bcl-2 and p53AIP1 is greater than their dissociation rate [15]. The irreversible activation of Casp3 is characterized with a bistable switch because of the positive feedback between CytoC release and Casp3 activation [16].

Appendix: Equations of the model

$$
\begin{aligned}
[\mathrm{ATM}] &= \mathrm{ATM_{tot}} - 2[\mathrm{ATM_d}] - [\mathrm{ATM_p}] && (1)\\
\frac{d[\mathrm{ATM_p}]}{dt} &= k_{\mathrm{acatm}}\frac{N_\mathrm{C}}{N_\mathrm{C}+j_{\mathrm{nc}}}[\mathrm{ATM_p}]\frac{[\mathrm{ATM}]}{[\mathrm{ATM}]+j_{\mathrm{acatm}}} \\
&\quad -k_{\mathrm{deatm}}(1+[\mathrm{Wip1}])\frac{[\mathrm{ATM_p}]}{[\mathrm{ATM_p}]+j_{\mathrm{deatm}}} && (2)\\
\frac{d[\mathrm{ATM_d}]}{dt} &= 0.5k_{\mathrm{dim}}[\mathrm{ATM}]^2 - k_{\mathrm{undim}}[\mathrm{ATM_d}] && (3)\\
\frac{d[\mathrm{p53_p}]}{dt} &= k_{\mathrm{acp53}}[\mathrm{p53}] - k_{\mathrm{dep53}}[\mathrm{p53_p}] - k_{\mathrm{dp53p}}[\mathrm{Mdm2_n}]\frac{[\mathrm{p53_p}]}{[\mathrm{p53_p}]+j_{\mathrm{1p53n}}} && (4)\\
\frac{d[\mathrm{p53}]}{dt} &= k_{\mathrm{sp53}} - k_{\mathrm{dp53n}}[\mathrm{p53}] + k_{\mathrm{dep53}}[\mathrm{p53_p}] - k_{\mathrm{acp53}}[\mathrm{p53}] \\
&\quad -k_{\mathrm{dp53}}[\mathrm{Mdm2_n}]\frac{[\mathrm{p53}]}{[\mathrm{p53}]+j_{\mathrm{1p53n}}} && (5)\\
k_{\mathrm{acp53}} &= k_{\mathrm{acp530}}\frac{[\mathrm{ATM_p}]}{[\mathrm{ATM_p}]+j_{\mathrm{atm}}} && (6)\\
k_{\mathrm{dmdm2n}} &= k_{\mathrm{dmdm2n0}} + k_{\mathrm{dmdm2n1}}\frac{[\mathrm{ATM_p}]}{[\mathrm{ATM_p}]+j_{\mathrm{atm}}} && (7)\\
\frac{d[\mathrm{mdm2m}]}{dt} &= k_{\mathrm{smdm2m0}} + k_{\mathrm{smdm2m}}\frac{[\mathrm{p53_p}]^4}{[\mathrm{p53_p}]^4+j_{\mathrm{p53}}^4} - k_{\mathrm{dmdm2m}}[\mathrm{mdm2m}] && (8)\\
\frac{d[\mathrm{Mdm2_n}]}{dt} &= k_{\mathrm{i}}[\mathrm{Mdm2_{cp}}] - k_{\mathrm{o}}[\mathrm{Mdm2_n}] - k_{\mathrm{dmdm2n}}[\mathrm{Mdm2_n}] && (9)\\
\frac{d[\mathrm{Mdm2_c}]}{dt} &= k_{\mathrm{tmdm2}}[\mathrm{mdm2m}] - k_{\mathrm{dmdm2c}}[\mathrm{Mdm2_c}] + k_{\mathrm{dpmdm2}}\frac{[\mathrm{Mdm2_{cp}}]}{[\mathrm{Mdm2_{cp}}]+j_{\mathrm{dpmdm2}}} \\
&\quad -k_{\mathrm{pmdm2}}[\mathrm{Akt_p}]\frac{[\mathrm{Mdm2_c}]}{[\mathrm{Mdm2_c}]+j_{\mathrm{pmdm2}}} && (10)\\
k_{\mathrm{tmdm2}} &= \frac{k_{\mathrm{tmdm20}}}{1+[\text{miR-605}]} && (11)\\
\frac{d[\mathrm{Mdm2_{cp}}]}{dt} &= k_{\mathrm{pmdm2}}[\mathrm{Akt_p}]\frac{[\mathrm{Mdm2_c}]}{[\mathrm{Mdm2_c}]+j_{\mathrm{pmdm2}}} - k_{\mathrm{dpmdm2}}\frac{[\mathrm{Mdm2_{cp}}]}{[\mathrm{Mdm2_{cp}}]+j_{\mathrm{dpmdm2}}} \\
&\quad -k_{\mathrm{i}}[\mathrm{Mdm2_{cp}}] + k_{\mathrm{o}}[\mathrm{Mdm2_n}] - k_{\mathrm{dmdm2c}}[\mathrm{Mdm2_{cp}}] && (12)\\
\frac{d[\text{miR-605}]}{dt} &= k_{\mathrm{smiR6050}} + k_{\mathrm{smiR605}}\frac{[\mathrm{p53_p}]^4}{[\mathrm{p53_p}]^4+j_{\mathrm{smiR605}}^4} - k_{\mathrm{dmiR605}}[\text{miR-605}] && (13)\\
\frac{d[\mathrm{Akt_p}]}{dt} &= k_{\mathrm{acakt}}[\mathrm{PIP3}]\frac{[\mathrm{Akt}]}{[\mathrm{Akt}]+j_{\mathrm{acakt}}} - k_{\mathrm{deakt}}\frac{[\mathrm{Akt_p}]}{[\mathrm{Akt_p}]+j_{\mathrm{deakt}}} && (14)\\
[\mathrm{Akt}] &= \mathrm{Akt_{tot}} - [\mathrm{Akt_p}] && (15)\\
\frac{d[\mathrm{PIP3}]}{dt} &= k_{\mathrm{p2}}\frac{[\mathrm{PIP2}]}{[\mathrm{PIP2}]+j_{\mathrm{p2}}} - k_{\mathrm{p3}}[\mathrm{PTEN}]\frac{[\mathrm{PIP3}]}{[\mathrm{PIP3}]+j_{\mathrm{p3}}} && (16)\\
[\mathrm{PIP2}] &= \mathrm{PIP_{tot}} - [\mathrm{PIP3}] && (17)
\end{aligned}
$$

$$\frac{d[\text{p53-killer}]}{dt} = k_{\text{p46}}[\text{p53DINP1}]\frac{[\text{p53-arrester}]}{[\text{p53-arrester}]+j_{\text{p46}}} - k_{\text{dp46}}[\text{Wip1}]\frac{[\text{p53-killer}]}{[\text{p53-killer}]+j_{\text{dp46}}} \quad (18)$$

$$[\text{p53-arrester}] = [\text{p53}_{\text{p}}] - [\text{p53-killer}] \quad (19)$$

$$\frac{d[\text{Wip1}]}{dt} = k_{\text{swip10}} + k_{\text{swip1}}\frac{[\text{p53-arrester}]^4}{[\text{p53-arrester}]^4+j_{\text{swip1}}^4} - k_{\text{dwip1}}[\text{Wip1}] \quad (20)$$

$$\frac{d[\text{p21}]}{dt} = k_{\text{sp210}} + k_{\text{sp21}}\frac{[\text{p53-arrester}]^4}{[\text{p53-arrester}]^4+j_{\text{sp21}}^4} - k_{\text{dp21}}[\text{p21}] \quad (21)$$

$$\frac{d[\text{miR-34a}]}{dt} = k_{\text{smiR34a0}} + k_{\text{smiR34a}}\frac{[\text{p53}_{\text{p}}]^4}{[\text{p53}_{\text{p}}]^4+j_{\text{smiR34a}}^4} - k_{\text{dmiR34a}}[\text{miR-34a}] \quad (22)$$

$$\frac{d[\text{p53DINP1}]}{dt} = k_{\text{sdinp10}} + k_{\text{sdinp11}}\frac{[\text{p53-arrester}]^4}{[\text{p53-arrester}]^4+j_{\text{sdinp11}}^4} + k_{\text{sdinp12}}\frac{[\text{p53-killer}]^4}{[\text{p53-killer}]^4+j_{\text{sdinp12}}^4} - k_{\text{ddinp1}}[\text{p53DINP1}] \quad (23)$$

$$\frac{d[\text{Bcl2}_{\text{tot}}]}{dt} = k_{\text{sbcl2tot}}\frac{j_{\text{sbcl2tot}}}{j_{\text{sbcl2tot}}+[\text{miR-34a}]} - k_{\text{dbcl2tot}}[\text{Bcl2}_{\text{tot}}] \quad (24)$$

$$[\text{Bcl2}] = [\text{Bcl2}_{\text{tot}}] - [\text{p53AIP1}\cdot\text{Bcl2}] \quad (25)$$

$$\frac{d[\text{p53AIP1}_{\text{tot}}]}{dt} = k_{\text{saip1tot0}} + k_{\text{saip1tot}}\frac{[\text{p53-killer}]^4}{[\text{p53-killer}]^4+j_{\text{saip1tot}}^4} - k_{\text{daip1tot}}[\text{p53AIP1}_{\text{tot}}] \quad (26)$$

$$[\text{p53AIP1}] = [\text{p53AIP1}_{\text{tot}}] - [\text{p53AIP1}\cdot\text{Bcl2}] \quad (27)$$

$$\frac{d[\text{p53AIP1}\cdot\text{Bcl2}]}{dt} = k_{\text{sp53ab}}[\text{p53AIP1}][\text{Bcl2}] - k_{\text{dp53ab}}[\text{p53AIP1}\cdot\text{Bcl2}] \quad (28)$$

$$\frac{d[\text{PTEN}]}{dt} = k_{\text{sPTEN0}} + k_{\text{sPTEN}}\frac{[\text{p53-killer}]^4}{[\text{p53-killer}]^4+j_{\text{sPTEN}}^4} - k_{\text{dPTEN}}[\text{PTEN}] \quad (29)$$

$$\frac{d[\text{Casp3}]}{dt} = (k_{\text{accasp30}} + k_{\text{accasp31}}\frac{[\text{CytoC}]^4}{[\text{CytoC}]^4+j_{\text{cytoc}}^4})(\text{Casp3}_{\text{tot}} - [\text{Casp3}]) - k_{\text{decasp3}}[\text{Casp3}] \quad (30)$$

$$\frac{d[\text{CytoC}]}{dt} = (k_{\text{accytoc0}} + k_{\text{accytoc1}}[\text{p53AIP1}]\frac{[\text{Casp3}]^4}{[\text{Casp3}]^4+j_{\text{casp3}}^4})(\text{CytoC}_{\text{tot}} - [\text{CytoC}]) - k_{\text{decytoC}}[\text{CytoC}] \quad (31)$$

[1] Xiao, J., H. Lin, X. Luo, X. Luo, and Z. Wang. 2011. miR-605 joins p53 network to form a p53:miR-605:Mdm2 positive feedback loop in response to stress. *EMBO J.* 30:524-532.

[2] Hermeking, H. 2010. The miR-34 family in cancer and apoptosis. *Cell Death Differ.* 17:193-199.

[3] Rothkamm, K., I. Kruger, L. H. Thompson, and M. Lobrich. 2003. Pathways of DNA double-strand break repair during the mammalian cell cycle. *Mol. Cell Biol.* 23:5706-5715.

[4] Stewart, R. D. 2001. Two-lesion kinetic model of double-strand break rejoining and cell killing. *Radiat. Res.* 156:365-378.

[5] Ma, L., J. Wagner, J. J. Rice, W. Hu, A. J. Levine, and G. A. Stolovitzky. 2005. A plausible model for the digital response of p53 to DNA damage. *Proc. Natl. Acad. Sci. USA.* 102:14266-14271.

[6] Zhang, X. P., F. Liu, and W. Wang. 2011. Two-phase dynamics of p53 in the DNA damage response. *Proc. Natl. Acad. Sci. USA.* 108:8990-8995.

[7] Zhang, X. P., F. Liu, Z. Cheng, and W. Wang. 2009. Cell fate decision mediated by p53 pulses. *Proc. Natl. Acad. Sci. USA.* 106:12245-12250.

[8] Bakkenist, C. J., and M. B. Kastan. 2003. DNA damage activates ATM through intermolecular autophosphorylation and dimer dissociation. *Nature.* 421:499-506.

[9] Shreeram, S., O. N. Demidov, W. K. Hee, H. Yamaguchi, N. Onishi, C. Kek, O. N. Timofeev, C. Dudgeon, A. J. Fornace, C. W. Anderson, Y. Minami, E. Appella, and D. V. Bulavin. 2006. Wip1 phosphatase modulates ATM-dependent signaling pathways. *Mol. Cell.* 23:757-764.

[10] Jeffrey, P., S. Gorina, and N. Pavletich. 1995. Crystal structure of the tetramerization domain of the p53 tumor suppressor at 1.7 angstroms. *Science.* 267:1498-1502.

[11] Lavin, M. F., and N. Gueven. 2006. The complexity of p53 stabilization and activation. *Cell Death Differ.* 13:941-950.

[12] Mayo, L. D., and D. B. Donner. 2001. A phosphatidylinositol 3-kinase/Akt pathway promotes translocation of Mdm2 from the cytoplasm to the nucleus. *Proc. Natl. Acad. Sci. USA.* 98:11598-11603.

[13] Gottlieb, T. M., J. F. Leal, R. Seger, Y. Taya, and M. Oren. 2002. Cross-talk between Akt, p53 and Mdm2: possible implications for the regulation of apoptosis. *Oncogene.* 21:1299-1303.

[14] Okamura, S., H. Arakawa, T. Tanaka, H. Nakanishi, C. C. Ng, Y. Taya, M. Monden, and Y.

Nakamura. 2001. p53DINP1, a p53-inducible gene, regulates p53-dependent apoptosis. *Mol. Cell.* 8:85-94.

[15] Matsuda, K., K. Yoshida, Y. Taya, K. Nakamura, Y. Nakamura, and H. Arakawa. 2002. p53AIP1 regulates the mitochondrial apoptotic pathway. *Cancer Res.* 62:2883-2889.

[16] Kirsch, D. G., A. Doseff, B. N. Chau, D. S. Lim, N. C. de Souza-Pinto, R. Hansford, M. B. Kastan, Y. A. Lazebnik, and J. M. Hardwick. 1999. Caspase-3-dependent cleavage of Bcl-2 promotes release of cytochrome c. *J. Biol. Chem.* 274:21155-21161.

SUPPLEMENTAL TABLE S1: DESCRIPTION OF VARIABLES AND THEIR INITIAL VALUES

Variable	Description	Initial value
$[ATM_d]$	Concentration of ATM dimer	1.0
$[ATM_p]$	Concentration of phosphorylated ATM monomer	0.1
[p53]	Concentration of inactive p53	0.0458
$[p53_p]$	Concentration of phosphorylatd p53	0.0
[mdm2m]	Concentration of mdm2 mRNA	0.0
$[Mdm2_c]$	Concentration of cytoplasmic Mdm2	0.1113
$[Mdm2_{cp}]$	Concentration of phosphorylated cytoplasmic Mdm2	0.4442
$[Mdm2_n]$	Concentration of nuclear Mdm2	0.1
$[Akt_p]$	Concentration of active Akt	0.121
[PIP3]	Concentration of PIP3	0.01
[p53-arrester]	Concentration of p53 phosphorylated at Ser15	0.001
[p53-killer]	Concentration of p53 phosphorylated at Ser15 and Ser46	0.001
[p21]	Concentration of p21	0.0
[Wip1]	Concentration of wild-type p53 induced protein 1	0.2
[PTEN]	Concentration of phosphatase and tensin homolog	0.01
[p53DINP1]	Concentration of p53-dependent damage-inducible protein 1	0.001
$[p53AIP1_{tot}]$	Total concentration of p53-regulated apoptosis-inducing protein 1	0.1
[CytoC]	Concentration of active cytochrome c	0.06
[Casp3]	Concentration of active caspase-3	0.05
[miR-605]	Concentration of miR-605	0.05
[miR-34a]	Concentration of miR-34a	0.05
$[Bcl2_{tot}]$	Total concentration of Bcl-2	2.2
[Bcl-2]	Concentration of active Bcl-2	2.2
[p53AIP1·Bcl2]	Concentration of p53AIP1 in complex with Bcl-2	0.0

SUPPLEMENTAL TABLE S2: STANDARD PARAMETERS OF THE MODEL

Rate Constant	Description	Value	Reference
N_{RP}	Number of repair proteins	20	[5,6]
k_{fb1}	Association rate of repair proteins in fast kinetics	1.3	[5,6]
k_{fb2}	Association rate of repair proteins in slow kinetics	0.13	[5,6]
k_{rb1}	Dissociation rate of repair proteins in fast kinetics	0.3	[5,6]
k_{rb2}	Dissociation rate of repair proteins in slow kinetics	0.03	[5,6]
k_{fix1}	DSB ligation rate in fast kinetics	0.02	[5,6]
k_{fix2}	DSB ligation rate in slow kinetics	0.002	[5,6]
k_{cross}	DSB binary mismatch rate	0.0007	[5,6]
k_{dim}	ATM dimerization rate	10.0	[5,6]
k_{undim}	ATM undimerization rate	1.0	[5,6]
k_{acatm}	ATM activation rate	2.0	[5,6]
k_{deatm}	ATM inactivation rate	1.3	[5,6]
j_{acatm}	Michaelis constant of ATM activation	1.0	[5,6]
j_{deatm}	Michaelis constant of $\mathrm{ATM_p}$ inactivation	2.3	[5,6]
j_{nc}	Threshold number of DSBC for ATM activation	1.0	[5,6]
$\mathrm{ATM_{tot}}$	Total concentration of all forms of ATM	5.0	[5,6]
j_{atm}	Michaelis constant of $\mathrm{ATM_p}$ as a kinase	1.0	[6]
k_{smdm2m0}	Basal induction rate of mdm2 mRNA	0.0018	[5]
k_{smdm2m}	p53-dependent transcription rate of mdm2	0.024	[5]
k_{dmdm2m}	Degradation rate of mdm2 mRNA	0.02	[5]
k_{tmdm2m0}	Translation rate of mdm2 mRNA	0.02	[5]
k_{dmdm2n0}	Basel degradation rate of nuclear Mdm2	0.003	[5,6]
k_{dmdm2n1}	ATM-dependent degradation rate of nuclear Mdm2	0.05	[5,6]
k_{dmdm2c}	Degradation rate of cytoplasmic Mdm2	0.003	[6]
k_{dpmdm2}	Dephosphorylation rate of cytoplasmic Mdm2	0.3	[6]
j_{dpmdm2s}	Michaelis constant of Mdm2 dephosphorylation	0.1	[6]
k_{pmdm2}	Akt-dependent phosphorylation rate of cytoplasmic Mdm2	8.0	[6]

j_{pmdm2}	Michaelis constant of Akt-dependent Mdm2 phosphorylation	0.3	[6]
k_{i}	Nuclear import rate of $\mathrm{Mdm2_{cp}}$	0.06	[6]
k_{o}	Nuclear export rate of $\mathrm{Mdm2_{n}}$	0.09	[6]
k_{smiR6050}	Basal induction rate of miR-605	0.002	Estimated
k_{smiR605}	p53-dependent induction rate of miR-605	0.02	Estimated
j_{smiR605}	Michaelis constant of p53-dependent miR-605 production	1.0	Estimated
k_{dmiR605}	Degradation rate of miR-605	0.02	Estimated
k_{smiR34a0}	Basal induction rate of miR-34a	0.002	Estimated
k_{smiR34a}	p53-inducible production rate of miR-34a	0.02	Estimated
j_{smiR34a}	Michaelis constant of p53-inducible miR-34a production	1.0	Estimated
k_{dmiR34a}	Degradation rate of miR-34a	0.02	Estimated
k_{acp530}	ATM-dependent activation rate of p53	0.2	[5,6]
k_{dep53}	Dephosphorylation rate of p53	0.1	[5,6]
k_{dp53p}	Mdm2-dependent degradation rate of $\mathrm{p53_{p}}$	0.01	[5,6]
k_{sp53}	Production rate of p53	0.2	[5,6]
k_{dp53n}	Basal degradation rate of p53	0.05	[5,6]
k_{dp53}	Mdm2-dependent degradation rate of p53	0.7	[5,6]
j_{1p53n}	Michaelis constant of Mdm2-dependent p53 degradation	0.1	[6]
j_{p53}	Michaelis constant of p53-dependent mdm2 mRNA production	1.0	[6]
k_{acakt}	Phosphorylation rate of Akt	0.25	[6]
j_{acakt}	Michaelis constant of Akt phosphorylation	0.1	[6]
k_{deakt}	Dephosphorylation rate of $\mathrm{Akt_{p}}$	0.1	[6]
j_{deakt}	Michaelis constant of $\mathrm{Akt_{p}}$ dephosphorylation	0.2	[6]
k_{p2}	Phosphorylation rate of PIP2	0.1	[6]
j_{p2}	Michaelis constant of PIP2 phosphorylation	0.2	[6]
k_{p3}	PTEN-dependent dephosphorylation rate of PIP3	0.5	[6]
j_{p3}	Michaelis constant of PIP3 dephosphorylation	0.4	[6]
$\mathrm{PIP_{tot}}$	Total concentration of PIP2 and PIP3	1.0	[6,8]
$\mathrm{Akt_{tot}}$	Total concentration of Akt	1.0	[6]

k_{p46}	Rate constant of p53 arrester phosphorylation	0.6	[6]
j_{p46}	Michaelis constant of p53-arrester phosphorylation	0.5	[6]
k_{dp46}	Rate constant of p53-killer dephosphorylation	0.3	[6]
j_{dp46}	Michaelis constant of p53-killer dephosphorylation	0.2	[6]
k_{swip10}	Basal induction rate of Wip1	0.01	[6]
k_{swip1}	p53-arrester inducible production rate of Wip1	0.073	Estimated
j_{swip1}	Michaelis constant of p53-dependent Wip1 production	0.5	[6]
k_{dwip1}	Degradation rate of Wip1	0.05	[6]
k_{sdinp10}	Basal induction rate of p53DINP1	0.001	[6]
k_{sdinp11}	p53-arrester inducible production rate of p53DINP1	0.009	[6]
j_{sdinp11}	Michaelis constant of p53-arrester dependent p53DINP1 production	0.7	[6]
k_{sdinp12}	p53-killer inducible production rate of p53DINP1	0.06	[6]
j_{sdinp12}	Michaelis constant of p53-killer dependent p53DINP1 production	0.3	[6]
k_{ddinp1}	Degradation rate of p53DINP1	0.01	[6]
k_{sPTEN0}	Basal induction rate of PTEN	0.01	[6]
k_{sPTEN}	p53-killer inducible production rate of PTEN	0.5	[6]
j_{sPTEN}	Michaelis constant of p53-dependent PTEN production	2.5	[6]
k_{dPTEN}	Degradation rate of PTEN	0.1	[6]
k_{sp210}	Basal induction rate of p21	0.01	[6]
k_{sp21}	p53-arrester inducible production rate of p21	0.2	[6]
j_{sp21}	Michaelis constant of p53-arrester inducible p21 production	0.6	[6]
k_{dp21}	Degradation rate of p21	0.1	[6]
$k_{\mathrm{saip1tot0}}$	Basal induction rate of p53AIP1	0.01	[6]
k_{saip1tot}	p53-killer inducible production rate of p53AIP1	0.32	[6]
j_{saip1tot}	Michaelis constant of p53-killer dependent p53AIP1 production	3.0	[6]
k_{daip1tot}	Degradation rate of p53AIP1	0.1	[6]
k_{accytoc0}	Basal release rate of mitochondrial cytochrome c	0.001	[6]
k_{accytoc1}	p53AIP1-dependent release rate of mitochondrial cytochrome c	0.9	[6]
j_{casp3}	Michaelis constant of caspase-3 dependent cytochrome c release	0.5	[6]

k_{decytoc}	Mitochondrial influx rate of cytochrome c	0.05	[6]
$\mathrm{CytoC}_{\mathrm{tot}}$	Total concentration of cytochrome c	3.0	[6]
$\mathrm{Casp3}_{\mathrm{tot}}$	Total concentration of caspase-3	3.0	[6]
k_{accasp30}	Basal activation rate of caspase-3	0.001	[6]
k_{accasp31}	Activation rate of caspase-3	0.9	[6]
j_{cytoc}	Michaelis constant of cytochrome c dependent caspase-3 activation	0.5	[6]
k_{decasp3}	Inactivation rate of caspase-3	0.07	[6]
k_{sbcl2tot}	Production rate of Bcl-2	0.075	Estimated
k_{dbcl2tot}	Degradation rate of Bcl-2	0.03	Estimated
j_{sbcl2tot}	Michaelis constant of Bcl-2 as a kinase	1.5	Estimated
k_{p53ab}	Association rate of p53AIP1 and Bcl-2	0.2	Estimated
k_{dp53ab}	Dissociation rate of p53AIP1·Bcl2 complex	0.1	Estimated

SUPPLEMENTAL FIGURES

Supplemental Figure S1: Time courses of the levels of ATM_p, p53-arrester, p53-killer, Wip1, and PTEN (from top to bottom) at $D_{IR} = 2$ Gy (A) or 6 Gy (B).

Supplemental Figure S2: Histograms of the time required for caspase-3 activation at $D_{IR} = 6$ Gy in the two cases of $k_{smiR605} = 0.02$ (*black*) and $k_{smiR605} = 0$ (*blue*). 2000 cells are counted.

Supplemental Figure S3: Time courses of the levels of p53-arrester, p53-killer, miR-34a, Bcl-2, $Bcl2_{tot}$, p53AIP1·Bcl2, p53AIP1 and Casp3 at $D_{IR} = 6$ Gy with $k_{smiR34a} = 0.02$ (A) or 0 (B).

Supplemental Figure S4: Temporal evolution of $[p53_p]$ (*black*) and [Casp3] (*blue*) at $D_{IR} = 5$ Gy with $k_{smiR605} = 0$ and $k_{smiR34a} = 0.02$ (A) or $k_{smiR605} = 0.02$ and $k_{smiR34a} = 0$ (B). These traces are randomly chosen from those of 2000 cells.

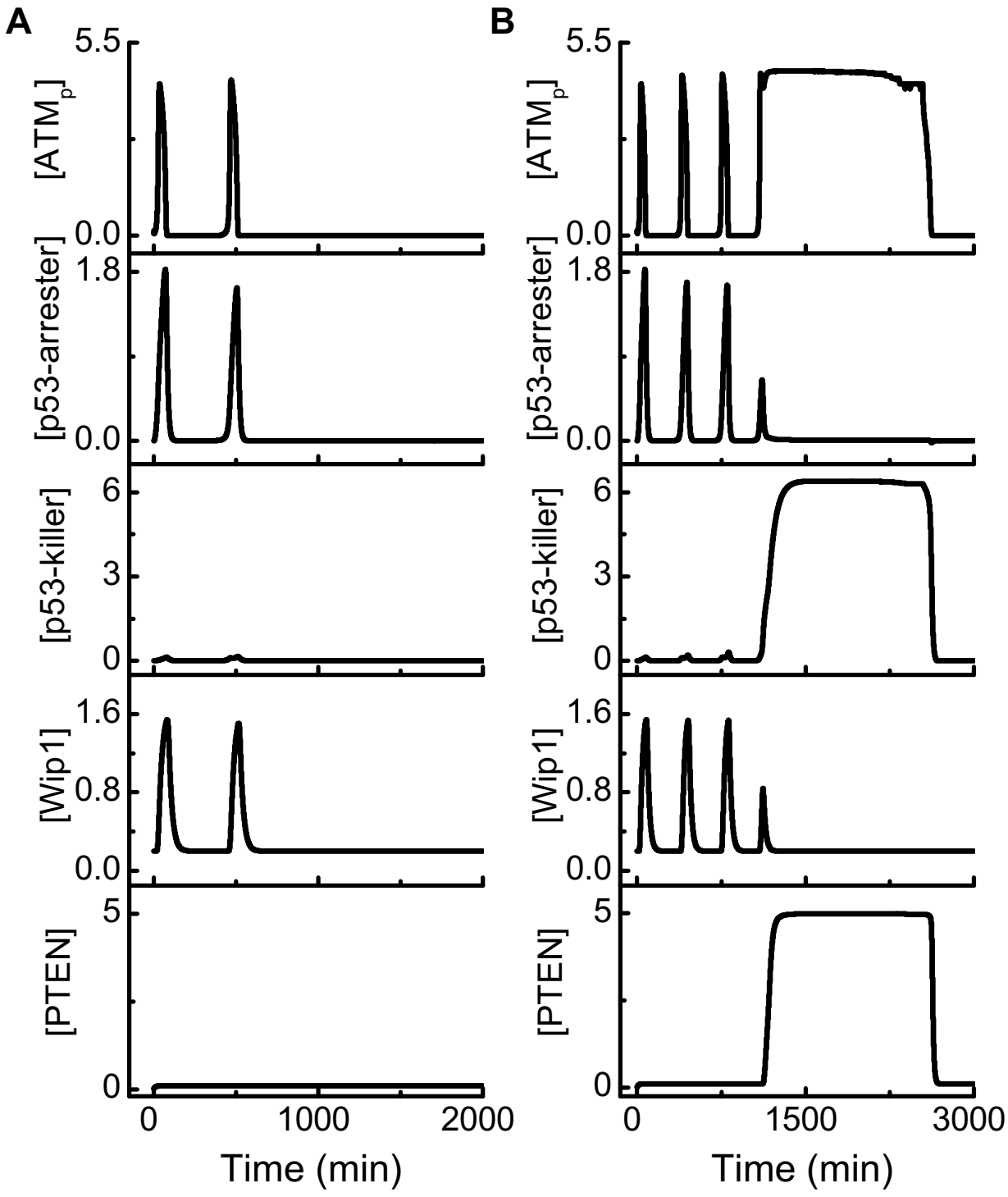

FIG. 1. Supplemental Figure S1

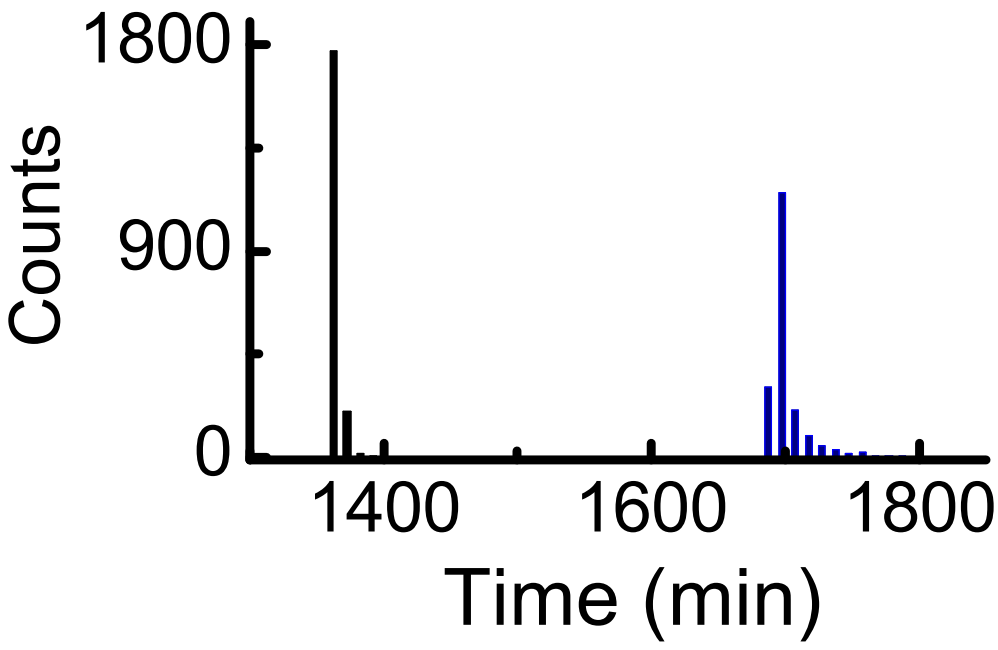

FIG. 2. Supplemental Figure S2

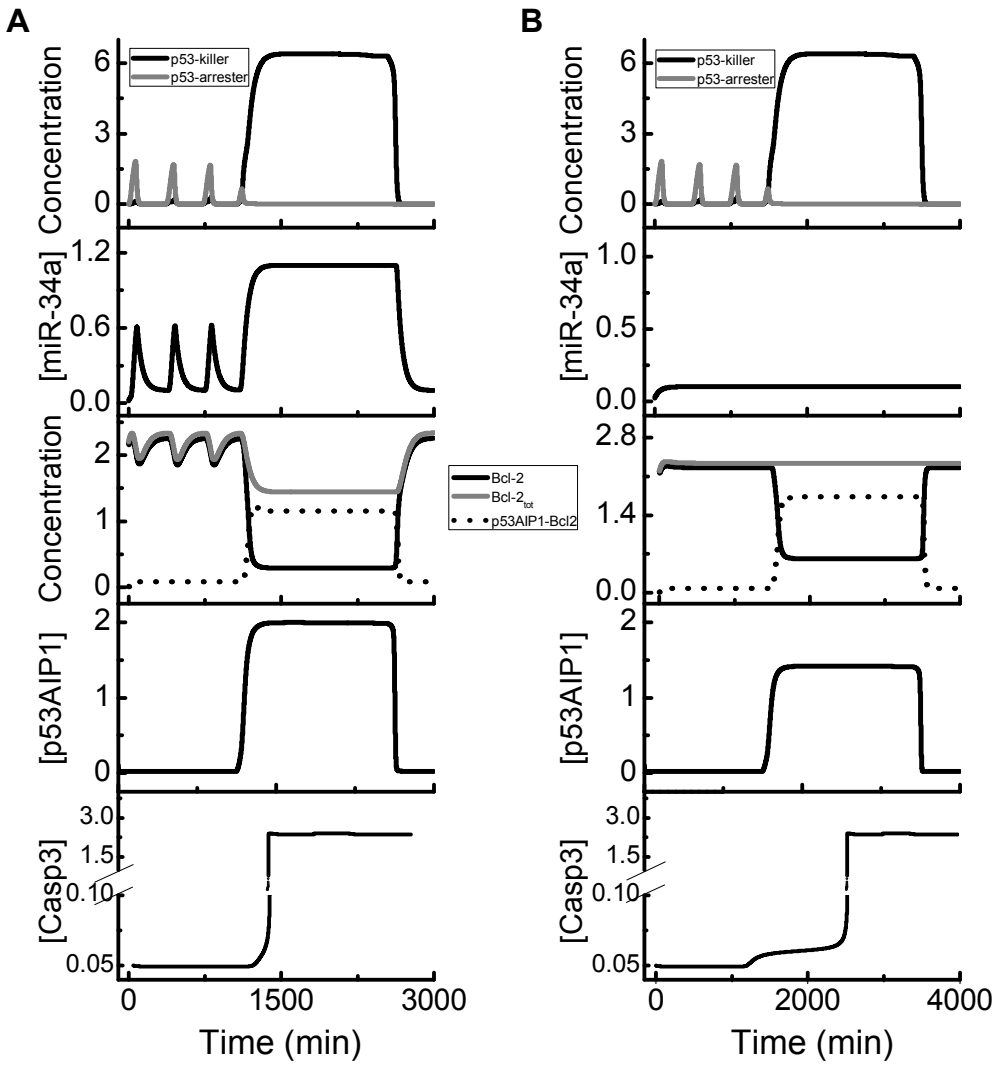

FIG. 3. Supplemental Figure S3

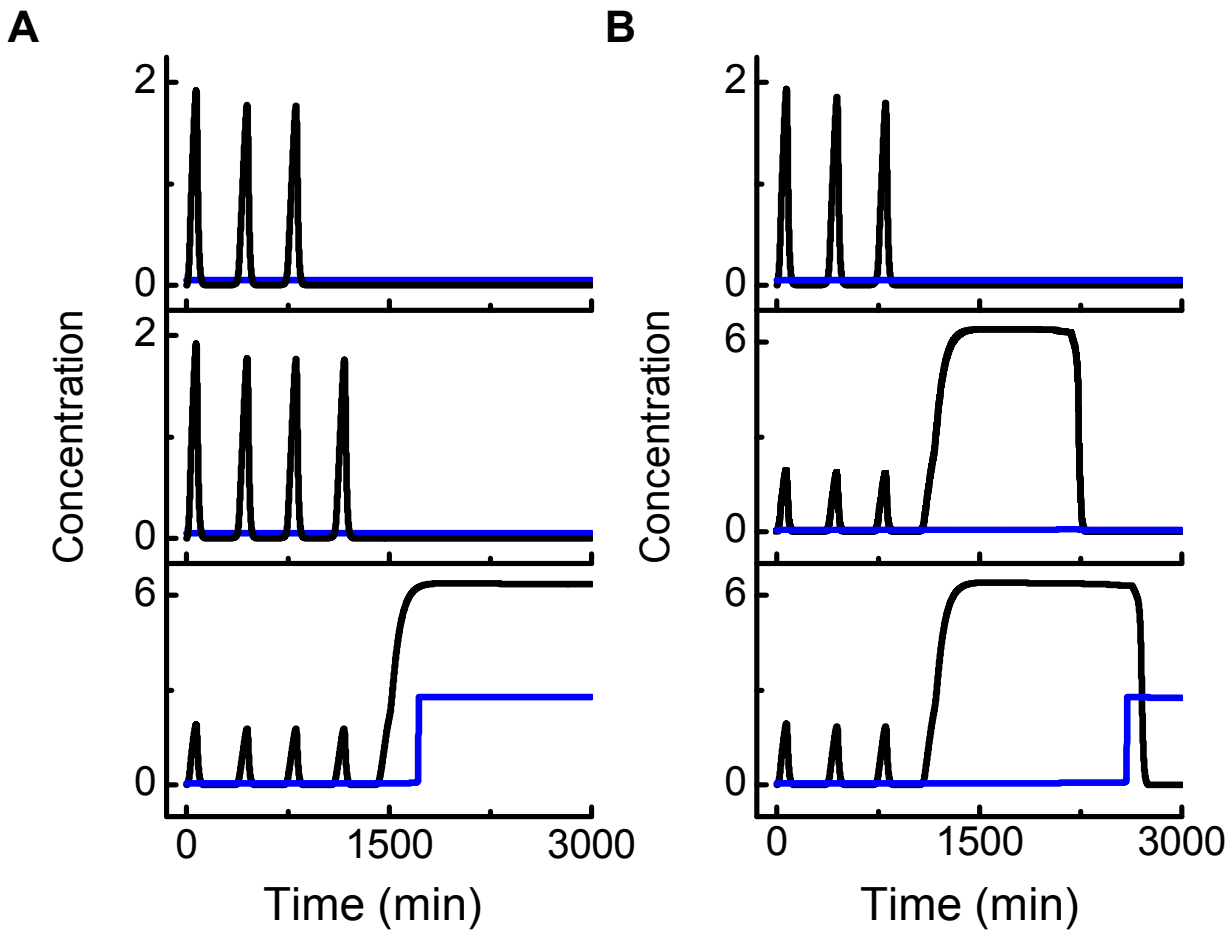

FIG. 4. Supplemental Figure S4